Published in final edited form as:
Nature. 2018 August ; 560(7716): 117–121. doi:10.1038/s41586-018-0340-7.

The Shieldin complex mediates 53BP1-dependent DNA repair

Sylvie M. Noordermeer[1,2,*], **Salomé Adam**[1,*], **Dheva Setiaputra**[1,*], **Marco Barazas**[3], **Stephen J. Pettitt**[4], **Alexanda K. Ling**[5], **Michele Olivieri**[1,6], **Alejandro Álvarez-Quilón**[1], **Nathalie Moatti**[1], **Michal Zimmermann**[1], **Stefano Annunziato**[3], **Dragomir B. Krastev**[4], **Feifei Song**[4], **Inger Brandsma**[4], **Jessica Frankum**[4], **Rachel Brough**[4], **Alana Sherker**[1,6], **Sébastien Landry**[1], **Rachel K. Szilard**[1], **Meagan M. Munro**[1], **Andrea McEwan**[1], **Théo Goullet de Rugy**[1], **Zhen-Yuan Lin**[1], **Traver Hart**[7], **Jason Moffat**[6,8], **Anne-Claude Gingras**[1,6], **Alberto Martin**[5], **Haico van Attikum**[2], **Jos Jonkers**[3], **Christopher J. Lord**[4], **Sven Rottenberg**[3,9], and **Daniel Durocher**[1,6,#]

[1]Lunenfeld-Tanenbaum Research Institute, Mount Sinai Hospital, 600 University Avenue, Toronto, ON, M5G 1X5, Canada [2]Department of Human Genetics, Leiden University Medical Center, Einthovenweg 20, 2333 ZC, Leiden, The Netherlands [3]Division of Molecular Pathology, Oncode Institute, Netherlands Cancer Institute, Plesmanlaan 121, 1066 CX Amsterdam, The Netherlands [4]The CRUK Gene Function Laboratory and Breast Cancer Now Toby Robins Research Centre, The Institute of Cancer Research, London, SW3 6JB, United Kingdom [5]Department of Immunology, University of Toronto, Medical Sciences Building, Toronto, ON M5S 1A8, Canada [6]Department of Molecular Genetics, University of Toronto, ON, M5S 1A8, Canada [7]Department of Bioinformatics and Computational Biology, University of Texas MD Anderson Cancer Center, Houston, Texas, USA [8]Donnelly Centre, University of Toronto, Toronto, ON, M5S 3E2, Canada [9]Institute of Animal Pathology, Vetsuisse Faculty, University of Bern, Laenggasstrasse 122, 3012 Bern, Switzerland

Abstract

[#]corresponding author.
[*]Co-first authors

Author contributions

SMN initiated the project in the DD lab, performed the RPE1 *BRCA1-KO* screen, validated hits and performed functional follow up. SAd performed validation and localization studies. DS carried out structure-function analyses and DNA binding studies. MB performed murine tumor model studies. SJP analyzed the SUM149PT talazoparib screen and validated hits. AL generated knockouts in CH12F3-2 cells, carried out CSR assays and analyzed AID levels. MO performed the IR screen and validation. AAQ carried out immunopurifications and helped with IF quantitation. NM performed CSR, TLR and pRPA assays. MZ carried out the SUM149PT olaparib screen and generated the RPE1 *BRCA1-KO* cells. SAn examined *Shld1* and *Shld2* mutations in mES cells. DK, IB, FS, JF and RB performed the SUM149PT talazoparib screen and validation. IB and FS developed SUM149PT knockout cells. FS carried out SUM149PT epistasis experiments. AS performed the REV7 IP-MS. SL initiated work on REV7. RKS generated vectors and edited the manuscript. MMM generated IP-MS cell lines. AMc carried out screen analysis, cloning and TIDE. TGR performed Shieldin qPCR. ZYL carried out IP-MS for SHLD1-3 under supervision of ACG. TH analyzed screen data and built the TKOv2 library with JM. AMa supervised AL. JJ and SR supervised MB and SAn. DD and HvA supervised SMN. CJL supervised SJP, DK, FS, IB, JF and RB. SMN and DD wrote the manuscript with input from the other authors.

Conflict of interest statement

DD and TH are advisors to Repare Therapeutics. CJL is a named inventor on patents describing the use of PARP inhibitors (DK3044221 (T3), ES2611504 (T3), US2014378525 (A1), WO2008020180 (A2), WO2009027650 (A1)) and stands to gain from their use as part of the ICR “Rewards to Inventors” scheme.

Europe PMC Funders Author Manuscripts

53BP1 is a chromatin-binding protein that regulates DNA double-strand break (DSB) repair by suppressing the nucleolytic resection of DNA termini1,2. This function of 53BP1 requires interactions with PTIP3 and RIF14–9, the latter also recruiting REV7/MAD2L2 to break sites10,11. How 53BP1-pathway proteins shield DNA ends is unknown but two models best explain their action: in one model, the 53BP1 complex strengthens the nucleosomal barrier to end-resection nucleases12,13, whereas in a second model, 53BP1 recruits effector proteins with end-protection activity. Here we describe the identification of such a 53BP1 effector complex, Shieldin, which includes C20orf196 (SHLD1), FAM35A (SHLD2), CTC-534A2.2 (SHLD3) and REV7. Shieldin localizes to DSB sites in a 53BP1- and RIF1-dependent manner and its SHLD2 subunit binds to ssDNA via OB-fold domains analogous to those of RPA1 and POT1. Loss of Shieldin impairs non-homologous end-joining (NHEJ), leads to defective immunoglobulin class switching and causes hyper-resection. Mutations in Shieldin subunit genes also cause resistance to poly(ADP-ribose) polymerase (PARP) inhibition in BRCA1-deficient cells and tumours due to restoration of homologous recombination (HR). Finally, we show that ssDNA binding by SHLD2 is critical for Shieldin function, consistent with a model where Shieldin protects DNA ends to mediate 53BP1-dependent DNA repair.

To discover proteins acting in the 53BP1 pathway, we searched for genes whose mutation restores HR in BRCA1-deficient cells leading to PARP inhibition resistance, a hallmark of 53BP1 deficiency14–16. We undertook three independent CRISPR/Cas9 screens that entailed the transduction of BRCA1-deficient cells with lentiviral libraries of single-guide (sg) RNAs (ED Fig 1a). The resulting pools of edited cells were exposed to near-lethal doses of two clinically used PARP inhibitors (PARPi), either olaparib or talazoparib17. We screened both an engineered human RPE1-hTERT *TP53*$^{-/-}$ *BRCA1*$^{-/-}$ cell line (hereafter referred to as RPE1 *BRCA1-KO*) and SUM149PT cells carrying a hemizygous *BRCA1* frameshift mutation. The gene-based results of the screens are found in Supplementary Table 1.

The genes coding for 53BP1 and for the uncharacterized protein C20orf196 were hits in all three screens (Fig 1a). We also identified *SCAF1* and *ATMIN*, which encode an SR-family protein and a transcription factor, respectively (Fig 1a). *PARP1* was a hit in the talazoparib-resistance screen, as expected18, whereas genes coding for proteins acting upstream (H2AX, MDC1, RNF8 and RNF168) or downstream (RIF1) of 53BP1, were hits in the RPE1 *BRCA1-KO* screen (Supplementary Table 1). The presence of 53BP1 and 53BP1-pathway proteins suggested that these screens could reveal hitherto uncharacterized 53BP1 effectors.

In competitive growth assays (Fig 1b), sgRNAs targeting *53BP1* led to outgrowth of *BRCA1-KO* cells in the presence of olaparib (Fig 1c; genotyping information in Supplementary Table 2). Similarly, sgRNAs targeting *C20orf196, ATMIN* and *SCAF1* led to PARPi resistance (Fig 1c and ED Fig 1b). In parallel studies, transfection of tracrRNA and crRNAs targeting *C20orf196*, *53BP1* or *PARP1* caused talazoparib resistance in SUM149PT cells (Fig 1d and ED Fig 1c). Since C20orf196 was identified as a hit in all three screens and validated in independent assays, we sought to determine its role in DNA repair.

C20orf196 is an uncharacterized protein of 205 amino acid residues (Fig 1e) previously identified as a candidate REV7-interacting protein19. We used immunoprecipitation coupled

to mass spectrometry (IP-MS) to expand the interaction network surrounding these proteins (Fig. 1f and Supplementary Table 3). One protein, FAM35A, was enriched in both C20orf196 and REV7 IP samples (Fig 1f). FAM35A was striking due to the presence of three predicted OB-fold domains (OBA, OBB and OBC; Fig 1e), reminiscent of those in the single-stranded (ss) DNA binding proteins RPA120 and POT121. FAM35A IP-MS experiments recovered CTC-534A2.2, also identified in the REV7 IP-MS (Fig. 1f and Supplementary Table 3). CTC-534A2.2 is a protein encoded by an alternative mRNA emanating from the *TRAPPC13* locus (Fig 1e and ED Fig 1d). sgRNAs against *CTC-534A2.2* were not present in either of our first-generation sgRNA libraries. IP-MS with CTC-534A2.2 recovered C20orf196, FAM35A and REV7 (Fig 1f and Supplementary Table 3), suggesting that these proteins form a single protein complex, which was confirmed by sequential affinity purification of epitope-tagged C20orf196, CTC-534A2.2, FAM35A and REV7 (Fig 1g).

FAM35A, *C20orf196* and *CTC-534A2.2* were identified in a fourth CRISPR/Cas9 screen employing a second-generation sgRNA library, TKOv2. This screen sought to identify genes promoting resistance to ionizing radiation (IR) in RPE1 cells (ED Fig 1e). 75 genes scored at a false discovery rate (FDR) <1% and this gene set was highly enriched in genes encoding NHEJ factors by gene ontology enrichment ($p= 1.11 \times 10^{-11}$, Fisher's exact test with multiple correction; Fig 2a and Supplementary Table 4). *RIF1*, *FAM35A*, *C20orf196*, *CTC-534A2.2*, *53BP1* and *REV7* were all hits at FDR <1% (Fig 2a). These data suggest that the complex formed by C20orf196, FAM35A, REV7 and CTC-534A2.2 promotes DSB repair by NHEJ. For reasons that will become apparent below, we named this complex Shieldin with C20orf196, FAM35A and CTC-534A2.2 renamed SHLD1, SHLD2 and SHLD3, respectively.

Independent sgRNAs targeting *SHLD2* or *SHLD3* caused sensitivity to the clastogen etoposide in competitive growth assays (ED Fig 1f) and caused resistance to olaparib in RPE1 *BRCA1-KO* cells, consistent with SHLD2/3 acting with REV7 and SHLD1 (Fig 2b and ED Fig 1g). Clonal knockouts of *SHLD1* or *SHLD2* led to olaparib resistance in *BRCA1-KO* cells, with the *SHLD2-KO* resulting in a phenotype that approached that of 53BP1 loss (Fig 2c). Similar results were obtained with 11 independent clonal knockouts of *SHLD1* in SUM149PT cells exposed to talazoparib (ED Fig 1h). Furthermore, expressing GFP-SHLD2 in *BRCA1-KO SHLD2-KO* cells restored olaparib sensitivity (ED Fig 1i). Resistance to PARPi in *BRCA1-KO* cells was likely due to restoration of HR, as measured both by RAD51 IR-induced focus formation and by a reporter for gene conversion, the traffic light reporter assay22 (Fig 2de and ED Fig 2a-d).

Next, we tested whether loss of Shieldin causes PARPi resistance in the KB1P mouse mammary tumor model deficient in *Brca1* and *Trp53* (p53)23. sgRNAs targeting *Shld1* and *Shld2* led to PARPi resistance in clonogenic survival assays in KB1P-G3 mammary tumor cells and in *Brca1*$^{-/-}$; *Trp53*$^{-/-}$ mouse embryonic stem (mES) cells (ED Fig 3ac). This resistance was also associated with restoration of HR (ED Fig 3b). Furthermore, transduction of *Shld1*- and *Shld2*-targeting sgRNAs suppressed the cell lethality associated with *Brca1* loss in p53-proficient mES cells (ED Fig 3d). We transduced the same sgRNAs into KB1P4 mammary tumor organoids (Supplementary Table 2) and implanted them into

the fat pads of mice. Olaparib treatment was initiated when tumors reached 50-100 mm^3 and was continued for 80 days. While all untreated mice succumbed to excessive tumour burden within 20 days, the control group responded to olaparib for the duration of the treatment (Fig 2f). However, mice implanted with *Shld1*- and *Shld2*-mutated tumours exhibited a partial response to olaparib, with mice succumbing by day 60 (Fig 2f). We conclude that Shieldin loss causes PARPi resistance in both human and mouse BRCA1-deficient tumour cells by reactivating HR.

As expected of a complex with a direct role in DSB repair, Shieldin accumulates at DSB sites in a 53BP1/RIF1-dependent manner (Fig 3a-f and ED Fig 4a-d). Loss of Shieldin components did not impair formation of 53BP1 or RIF1 IR-induced foci, indicating that Shieldin acts downstream of 53BP1-RIF1 (ED Fig 4e,f). Consistent with this possibility, we observed genetic epistasis between *53BP1* and the Shieldin genes using the RAD51 focus formation assay in RPE1 *BRCA1-KO cells* (ED Fig 5a). We also observed that *SHLD1* and *53BP1* were epistatic in terms of modulating talazoparib resistance in SUM149PT cells (ED Fig 5b).

Analyses of the dependencies within the Shieldin complex indicate that SHLD3 is the most apical component followed by REV7, SHLD2, and then SHLD1 (Fig 3c-e, ED Fig 4a-d, ED Fig 6, ED Fig 7c-e and Supplementary Document 1 for mapping details). Indeed, SHLD3 interacts with RIF1, suggesting that it recruits Shieldin to chromatin-bound 53BP1-RIF1 (Fig 3g and ED Fig 7f). Further mapping studies suggest that Shieldin consists of a DSB-recruitment module composed of SHLD3-REV7 that binds to the N-terminus of SHLD2 (residues 1-50; ED Fig 6, ED Fig 7a-c), and a presumptive DNA-binding module (SHLD2-SHLD1) featuring the OB-fold domains at the SHLD2 C-terminus (SHLD2C residues 421-904; ED Fig 7a).

To assess the role of Shieldin in NHEJ, we first analyzed class switch recombination (CSR) in CH12F3-2 cells24. Mutation of each of the Shieldin subunits compromised CSR, with *Shld1*-edited cells having a reproducibly milder phenotype (Fig 3h and ED Fig 8a-c). *Shld2-KO* was epistatic with both *53bp1-KO* and *Shld1-KO* mutations, consistent with them acting in the same genetic pathway (ED Fig 8bc). The expression of AID, which initiates CSR, was not altered in Shieldin mutants, consistent with NHEJ deficiency (ED Fig 8d). Supporting this possibility, *SHLD1* and *SHLD2* mutations impaired random plasmid integration, which occurs largely through NHEJ25, to an extent similar to that of 53BP1-deficient cells (ED Fig 8e,f).

Loss of each Shieldin subunit led to IR-induced RPA2 Ser4/Ser8 phosphorylation, a surrogate marker of end-resection20, suggesting that Shieldin protects DNA ends (Fig 3i and ED Fig 8g). Supporting this hypothesis, restoration of HR in Shieldin-defective KB1P-G3 cells was dependent on ATM activity (ED Fig 3ab), which promotes DNA end-resection in the absence of 53BP116 or REV710. In an accompanying paper, Mirman *et al.*26 show that *Shld2*-mutated cells have increased end-resection at dysfunctional telomeres. Shieldin therefore antagonizes end-resection.

We surmised that if Shieldin is a downstream effector of 53BP1, artificially targeting Shieldin to DSB sites should rescue phenotypes associated with 53BP1 loss. To do this, we fused SHLD2 to the RNF8 FHA domain, which is recruited to damaged chromatin independently of 53BP1 (Fig 4a). We found that the FHA-dependent targeting of SHLD2 to DSB sites suppressed RAD51 IR-induced focus formation in *BRCA1-KO 53BP1-KO* cells (Fig 4b and ED Fig 9a). These results suggest that SHLD2 mediates 53BP1-dependent DNA repair.

We observed that the FHA-SHLD2C protein, which contains the OB-fold domains, potently suppressed RAD51 recruitment to DSB sites in *BRCA1-KO 53BP1-KO* cells (Fig 4b and ED Fig 9a). This result suggested that DNA binding might underpin the effector function of the SHLD2 C-terminus. To test for DNA binding activity, we affinity-purified SHLD2C in the presence or absence of SHLD1 (ED Fig 9b). We observed SHLD2C binding to a radiolabeled ssDNA probe by electrophoretic mobility shift assays (EMSA), and competition with unlabeled oligonucleotides revealed that SHLD2C preferentially binds to ssDNA over dsDNA (Fig 4c). While SHLD1 is not essential for SHLD2C DNA-binding, its presence increased the amount of SHLD2C purified, and the retarded complex displayed a difference in mobility consistent with the SHLD2C-SHLD1 complex binding to ssDNA (Fig 4d, lanes 2 vs 5). We estimate the binding affinity of the SHLD2C-ssDNA interaction to be ~10 nM (Fig 4e and ED Fig 9c). We conclude that SHLD2 possesses ssDNA-binding activity.

To explore whether ssDNA-binding is involved in Shieldin function, we generated four mutant versions (m1-m4) of the SHLD2 OB-folds by modeling the SHLD2 C-terminus on an RPA1 structure (PDB 4GNX; ED Fig 9d)27. We also employed a splice variant of SHLD2 that disrupts OBB, which we refer to as SHLD2S. We found that the m1 and SHLD2S mutants, either in the context of full-length or SHLD2C proteins, were unable to suppress RAD51 focus formation in *BRCA1-KO 53BP1-KO* cells when fused to the RNF8 FHA domain (Fig 4b and ED Fig 9a). Expression of full-length SHLD2-m1 and SHLD2S in *BRCA1-KO SHLD2-KO* cells also failed to suppress RAD51 IR-induced focus formation, unlike wild-type SHLD2 (ED Fig 10ab). Importantly, both mutants localized to DSB sites (ED Fig 10cd) and interacted with the other members of the Shieldin complex (ED Fig 10e). Therefore, the SHLD2-m1 and SHLD2S mutants are defective in suppressing HR.

Strikingly, the SHLD2C-m1 mutant was completely defective in ssDNA binding (Fig 4d, lane 3) whereas the SHLD2C-S mutant displayed reduced and aberrant ssDNA-binding behaviour (Fig 4d, lane 4). Since the m1 mutation produces a protein defective both in ssDNA-binding and suppression of HR, but which is proficient in both complex assembly and DSB recruitment, we conclude that ssDNA binding by Shieldin is critical for 53BP1-dependent DSB repair.

In conclusion, the identification of Shieldin forces us to re-evaluate how DNA end stability is regulated in vertebrates. Indeed, our results are consistent with a model in which Shieldin is the ultimate mediator of 53BP1-dependent DNA repair by binding ssDNA and occluding access to resection nucleases (Fig 4f). Our discovery of Shieldin also has implications for

the management of *BRCA1*-mutated malignancies, as alterations in Shieldin-coding genes may cause clinical resistance to PARP inhibitors.

Methods

Plasmids

DNA corresponding to sgRNAs were cloned into pX330 (Addgene: 42230, Cambridge, MA, USA), LentiGuide-Puro (Addgene: 52963), LentiCRISPRv2 (Addgene: 52961), or a modified form in which Cas9 was replaced by NLS-tagged GFP or mCherry using *Age*I and *Bam*HI (designated as LentiGuide-NLS-GFP or –mCherry), as described29,30. Sequences of the sgRNAs used in this study are included in Supplementary Table 5. Coding sequences of C20orf196 and the short isoform of FAM35A were obtained from the ORFeome collection (horfdb.dfci.harvard.edu/), archived in the Lunenfeld-Tanenbaum Research Institute's OpenFreezer31. The complete coding sequence of the long isoform of FAM35A was generated by combining a synthesized fragment (GeneArt, Regensburg, Germany) corresponding to the long isoform C-terminus using an internal KpnI restriction site. The coding sequence of CTC534A2.2 was generated by gene synthesis (GeneArt). The coding sequences were PCR amplified using AscI and ApaI flanking primers and cloned into pcDNA5-FRT/TO-eGFP and pcDNA5-FRT/TO-Flag to obtain N-terminally tagged FAM35A, C20orf196 and CTC534A2.2. pGLUE-HA-Strep-FAM35A was generated by PCR amplification of the long isoform of FAM35A and cloning into pGLUE (Addgene: 15100) using *Asc*I and *Not*I. To generate FAM35A fragments and mutants, standard protocols for primer-directed mutagenesis or self-ligation of truncated PCR-products were used. To generate pcDNA5-FRT/TO-V5-CTC534A2.2, eGFP was replaced by a V5 tag in the cloning vector pcDNA5-FRT/TO-eGFP using *Kpn*I and *Asc*I restriction enzymes after which the coding sequence for CTC534A2.2 was PCR-amplified and inserted into pcDNA5-FRT/TO-V5-MCS using *Asc*I and *Xho*I restriction enzymes.

To generate RNF8-FHA fusions, the N-terminus of RNF8 (aa 1-160) was PCR amplified from pcDNA3-RNF8-FHA(1-160)-RNF168 with flanking AscI sites and inserted into pcDNA5-FRT/TO-eGFP-FAM35A. eGFP-(FHA-) fusions of FAM35A were introduced into pCW57.1 (Addgene: 41393) by Gateway cloning using the pDONR221 donor vector. FAM35A amino acid substitution mutations and deletions were introduced by site directed mutagenesis and deletion PCR, respectively.

The REV7 coding sequence was obtained from the ORFeome collection and was cloned into the pDEST-FRT/TO-eGFP vector using Gateway cloning and into the pcDNA5-FRT/TO-Flag vector by PCR amplification. The N-terminal 967 residues of RIF1 were amplified by PCR and cloned into the pDONR221 vector using Gateway technology. The fragment was then integrated into the pDEST-mCherry-LacR vector by Gateway cloning. Plasmids for the traffic light reporter system were obtained from Addgene (pCVL-TrafficLightReporter-Ef1a-Puro lentivirus: #31482; pCVL-SFFV-d14GFP-Ef1a-HA-NLS-Sce(opt)-T2A-TagBFP: #32627).

Cell lines and gene editing

293T and RPE1 hTERT cell lines were obtained from ATCC (Manassas, VA, USA), 293 Flp-In cells were obtained from Invitrogen (Carlsbad, CA, USA) and SUM149PT32 cells were obtained from Asterand Bioscience (Detroit, MI, USA). U2OS ER-mCherry-LacIFokI-DD cells (U2OS-265, referred to in the text as U2OS-FokI) were a kind gift of R. Greenberg (University of Pennsylvania, Philadelphia, PA, USA). All cell lines are routinely authenticated by STR-analysis and tested negative for mycoplasma. 293T, 293 Flp-In, U2OS and RPE1 cells were cultured in high glucose- and GlutaMAX-supplemented DMEM (Gibco, Thermo Fisher Scientific, Waltham, MA, USA) + 1% Penicillin / Streptomycin (Thermo Fisher Scientific) and 10% heat inactivated fetal calf serum (Wisent, St-Bruno, Canada) at 37ºC, 5% CO_2. SUM149PT cells were cultured in Ham's F12 medium (Gibco) supplemented with 5% FCS, 10 mM HEPES, 1 μg/mL hydrocortisone (Sigma-Aldrich, St. Louis, MI, USA), and 5 μg/mL insulin (Sigma-Aldrich) at 37ºC, 5% CO_2. Except for RPE1 clonogenic survival assays, which were performed at 3% O_2, cells were kept under normoxia conditions. Transient transfections of DNA and siRNA were performed using Lipofectamine 2000 (Thermo Fisher Scientific), PEI (Sigma-Aldrich) or calcium phosphate and Lipofectamine RNAiMAX, respectively (Thermo Fisher Scientific). siRNA efficiency was analysed by qPCR and immunoblotting. Stable integration of Flag-C20orf196/FAM35A/REV7 with the Flp-In system was achieved by co-transfection of the pcDNA5-FRT/TO plasmid with the recombinase vector pOG44 (Thermo Fisher Scientific) and hygromycin selection for integration. Lentiviral particles were produced in 293T cells by co-transfection of the targeting vector with vectors expressing VSV-G, RRE and REV using calcium phosphate or PEI (Sigma-Aldrich). Viral transductions were performed in the presence of 4-8 μg/μL polybrene (Sigma-Aldrich) at an MOI <1, unless stated otherwise. Transduced RPE1 cells were selected by culturing in the presence of 15 μg/mL puromycin. For the BRCA1-deficient mouse cell experiments, all experiments were performed using virus produced with the LentiCRISPRv2 backbone (see Supplementary Table 5) and cells were infected using polybrene (8 μg/mL). The medium was refreshed after 12 h and transduced cells were selected with puromycin.

The generation of RPE1 hTERT *TP53*$^{-/-}$ *BRCA1-KO* Cas9 cells has been described elsewhere (Zimmermann *et al.*, submitted). *REV7*, *53BP1*, *FAM35A* and *C20orf196* gene knockouts were generated by electroporation of LentiGuide or LentiCRISPRv2 vectors using a Lonza Amaxa II Nucleofector (Basel, Switzerland) (for sgRNA sequences employed see Supplementary Table 5; REV7 - sgRNA1, FAM35A - sgRNA2 and C20orf196 - sgRNA1 were used for clonal knockout generation). 24 h following transfection, cells were selected for 24-48 h with 15 μg/mL puromycin, followed by single clone isolation. Triple knockout cell lines of *TP53*, *BRCA1* and *53BP1* were created by mutating *BRCA1* from the *TP53*$^{-/-}$ *53BP1-KO* double knockout cell line. Triple knockout cell lines of *TP53*, *BRCA1* and *REV7*, *FAM35A* or *C20orf196* were created by mutating *REV7*, *FAM35A* or *C20orf196* in the *TP53*$^{-/-}$ *BRCA1-KO* cells. Loss of protein(s) was verified by immunoblotting when antibodies were available. Gene mutations were further confirmed by PCR amplification and TIDE analysis33 (for primers used for genomic PCR, see Supplementary Table 6, for genomic editing information, see Supplementary Table 2).

To generate SUM149PT *53BP1*, *PARP1* or *C20orf196* knockout populations of cells, SUM149PT-doxCAS9 cells were treated with doxycycline for 24 h at 1 μg/ml prior to transfection with EditR crRNA (Dharmacon, Lafayette, CO, USA). Transfection of guides 53BP1_5_1, 53BP1_5_3, PARP1_5_2, PARP1_5_4, C20orf196_5-1, C20orf196_5-2, C20orf196_5-3 and C20orf196_5-5 (see Supplementary Table 5) was performed at a concentration of 20 nM (crRNA:tracrRNA) in the presence of doxycycline (1 μg/ml) using Lipofectamine RNAiMAX in 48-well plates (35,000 cells per well). The following day cells were split 1:3, fed 24 h later with media supplemented with 50 nM talazoparib (without doxycycline) and kept in batch culture or further split to generate single cell colonies. Drug-containing media was replenished every 3-4 d until PARP inhibitor resistant pools or clones were established. Clones were subsequently picked, expanded and validated by genomic PCR and sequence analysis (for primers used, see Supplementary Table 6, for genomic editing information, see Supplementary Table 2). Four SUM149PT *C20orf196-KO* clones with mutations were chosen for further experimentation: clone A (C20orf196 5-1-C1), clone B (C20orf196 5-1-C2), clone C (C20orf196 5-3-C5) and clone D (C20orf196 5-5-C4).

To generate *53BP1-KO* double mutant clones, SUM149PT *C20orf196* clones A and D were infected with a lentivirus expressing an sgRNA targeting *TP53BP1* or a non-targeting control sgRNA (for sequences, see Supplementary Table 5) in media containing 1 μg/ml doxycycline. 48 h after infection, puromycin (1 μg/ml) was added to the media. Selection was maintained for 3 d, until the uninfected control cells were killed. Pools of selection-resistant cells were seeded into 384-well plates for short term survival assays (see below) or subcloned to generate clonal lines.

Mouse ES cells with a selectable conditional *Brca1* deletion ($Rosa26^{CreERT2/wt}$;$Brca1^{SCo/\Delta}$)34 were cultured on gelatin-coated plates in 60% buffalo red liver (BRL) cell-conditioned medium supplied with 10% fetal calf serum, 0.1 mM β-mercaptoethanol (Merck, Kenilworth, NJ, USA) and 10^3 U/ml ESGRO LIF (Millipore, Burlington, MA, USA) under normal oxygen conditions (21% O_2, 5% CO_2, 37 °C).

The KB1P-G3 2D cell line was previously established from a $Brca1^{-/-}$ $p53^{-/-}$ mouse mammary tumor and cultured as described14. Briefly, cells were cultured in DMEM/F-12 medium (Life Technologies, Carlsbad, CA, USA) in the presence of 10% FCS, penicillin/streptomycin (Gibco), 5 μg/mL insulin (Sigma-Aldrich), 5 ng/mL epidermal growth factor (Life Technologies) and 5 ng/mL cholera toxin (Gentaur, Kampenhout, Belgium) under low oxygen conditions (3% O_2, 5% CO^2 at 37 °C).

The KB1P4 3D tumor organoid line was previously established from a $Brca1^{-/-}$ $p53^{-/-}$ mouse mammary tumor and cultured as described35. Cells were seeded in Basement Membrane Extract Type 2 (BME, Trevigen, Gaithersburg, MD, USA) on 24-well suspension plates (Greiner Bio-One, Kremsmünster, Austria) and cultured in AdDMEM/F12 supplemented with 10 mM HEPES (Sigma-Aldrich), GlutaMAX (Invitrogen), penicillin/streptomycin (Gibco), B27 (Gibco), 125 μM N-acetyl-L-cysteine (Sigma-Aldrich), and 50 ng/mL murine epidermal growth factor (Invitrogen).

CH12F3-2 mutant clones were edited either through transient transfection with pX330 plasmid constructs expressing sgRNAs against *Trp53bp1* (sgRNA: *Trp53bp1*_e6_834, see Supplementary Table 5), *Fam35a*, and *Ctc534a2.2* or by lentiviral lentiCRISPR v2 transduction for *C20orf196*. Double knock-out cell lines of *Fam35a* and *Trp53bp1* or *C20orf196* were generated by transient transfection of a pX330 plasmid expressing an sgRNA against *Trp53bp1* or by lentiviral transduction with lentiCRISPRv2 with an sgRNA targeting *C20orf196*.

Antibodies, siRNAs and drugs

An overview of all the antibodies used in this study, including dilution factors, can be found in Supplementary Table 7. The following siRNAs from Dharmacon were used in this study (final siRNA concentration: 10 or 20nM): 53BP1: siRNA #2 (D-003548-02-0020); RIF1: siGENOME RIF1 siRNA (D-027983-02-0050); REV7: siGENOME MAD2L2 siRNA (M-003272-03-0010); C20orf196: SMARTpool: siGENOME C20orf196 siRNA (M-018767-00-0005); FAM35A: SMARTpool: siGENOME FAM35A siRNA (M-013761-01-0005); CTC534A2.2 (custom order): siRNA#1: 5'-GGACAAAACUCAAUCAAAU-3', siRNA#2: 5'-CAGUAGAUCUAUUGGAGUU-3', siRNA#3: 5'-CUGGAAGACAUUUGGACAA-3', siRNA#4: 5'-GCAAGAUAGUUUAAAGGCA-3' (used as a pool).

The following drugs were used in the course of this study: olaparib (SelleckChem, Houston, TX, USA, or Astra Zeneca, Cambridge, UK), talazoparib (SelleckChem), cisplatin (Sigma-Aldrich), the ATM-inhibitor KU60019 (Sigma-Aldrich), and etoposide (Sigma-Aldrich). Concentration and duration of treatment are indicated in the corresponding figure legends.

Olaparib resistance screens

Viral particles of the TKOv1 sgRNA library were produced as previously described36. This library contains 91,320 sgRNA sequences, with a modal number of six sgRNAs per gene. Cas9-expressing cells were infected with an MOI < 0.3 and the coverage of sgRNA representation was maintained at > 100x (SUM149PT) or > 200x (RPE1) (per replicate, if applicable). 24 h following transduction, transduced cells were selected for 120 h with 10 μg/mL puromycin (RPE1) or 48 h with 3 μg/mL puromycin, followed by 72 h with 0.5 μg/mL puromycin (SUM149PT). Three days after transduction, the transduced cells were split into three technical replicates. Cells were passaged once every three days until nine days after infection, at which time olaparib (16 nM for RPE1 *TP53*$^{-/-}$ *BRCA1-KO*, 2 μM for SUM149PT) was added to the cells. Olaparib-containing medium was refreshed every 4 d. Cells were harvested at 3, 9, 18 and 23 d post-infection (RPE1) or at 3, 9, 19 and 26 d post-infection (SUM149PT) for downstream processing as described36. In short, total genomic DNA was isolated from 2 x 10^7 (t3 sample) or 1 x 10^7 (later time points) cells using the QIAamp DNA Blood Maxi Kit (Qiagen, Germantown, MD, USA). DNA was precipitated with ethanol and sodium chloride and reconstituted in EB buffer (10 mM Tris-HCl pH 7.5). sgRNA sequences were PCR-amplified using primers harbouring Illumina TruSeq adapters with i5 and i7 barcodes, and the resulting libraries were sequenced on a Illumina NextSeq500 (San Diego, CA, USA) using parameters previously described36. Analysis was performed using Model-based Analysis of Genome-wide CRISPR-Cas9 Knockout

(MAGeCK) version 0.5.337, in conjunction with Python v3.5.1 on a Mac OS X El Capitan operating system. Non-treated samples collected at day 9 after transduction were compared to treated samples collected at day 23 (RPE1) or day 26 (SUM149PT). The positive score for each gene was calculated by using the 'run' function with the following arguments:

```
mageck run -l /path/to/TKOv1_library/ -n 08-02-2017_141703 --sample-label
test,CTRL -t 1 -c 0 --fastq /path/to/fastq1 /path/to/fastq2.
```

SUM149PT talazoparib resistance screen

A derivative of SUM149PT with an integrated tetracycline-inducible Cas9 expression allele was lentivirally infected with a genome-wide guide RNA library ("Yusa" library of 90,709 sgRNAs) designed to target 18,010 genes38, using a multiplicity of infection of 0.3 and infecting >1000 cells per sgRNA. After puromycin selection (3 μg/ml) to remove non-tranduced cells, a sample was removed (t0); remaining cells were cultured in the presence or absence of doxycycline plus 100 nM talazoparib, a concentration which normally results in complete inhibition of the cell population. No cells survived in the absence of doxycycline. After two weeks of selection, gDNA from the remaining cells in the doxycycline-treated sample was recovered. The sgRNA sequences from this gDNA were PCR-amplified using barcoded and tailed primers and deep sequenced to identify sgRNAs in the talazoparib-resistant population. sgRNA read data was analysed using a gene-level method (MaGeCK version 0.5.5) as well as using a normalised read frequency method to identify individual sgRNAs associated with resistance, by comparing sgRNA abundances in the resistant and starting populations.

Command used for read count generation:

```
mageck count --output-prefix PREFIX --list-seq
Human_genome_library_guides_for_mageck.csv --fastq T1.fastq T0.fastq --
sample-label T1,T0 --trim-5 0
```

Command used for MLE analysis:

```
mageck mle --norm-method none --output-prefix PREFIX --sgrna-eff-name-
column 3 --sgrna-eff-score-column 4 --sgrna-efficiency
annotation/sgrnas.bed --count-table pptm.counts.txt --design-matrix
designmatrix.txt
```

IR dropout screen and TKOv2 library

The TKOv2 lentiviral CRISPR library was used for whole-genome CRISPR knockout screening. To design TKOv2, all possible 20mer sequences upstream of NGG PAM sites were collected where the SpCas9 double-strand break would occur within a coding exon (defined by hg19/Gencode v19 "appris_principal," "appris_candidate_longest," or "appris_candidate" transcript). Guides with 40-75% GC content were retained and further filtered to exclude homopolymers of length ≥4, SNPs (dbSNP138), and relevant restriction sites, including *Bsm*I (GAATCG) and *Bsm*BI (CGTCTC). Candidate gRNA+PAM

sequences were mapped to hg19 and sequences with predicted off-target sites in exons or introns, or sequences with more than two predicted off-target sites (with up to two mismatches) in any location, were discarded. Remaining guides were scored using a "sequence score table" described previously39. Four guides per gene were selected, with a bias toward high sequence scores and maximal coverage across exons (i.e. moderate-scoring guides targeting different exons were preferred to high-scoring guides targeting the same exon). The final library contains 70,555 gRNA targeting 17,942 protein-coding genes, as well as 142 sequences targeting LacZ, luciferase, and eGFP. Oligo sequences were ordered from CustomArray (Bothell, WA), PCR-amplified, and cloned into the pLCKO vector as previously described36.

hTERT RPE1 *TP53*$^{-/-}$ Cas9-expressing cells were transduced with the lentiviral TKOv2 library (see below) at a low MOI (~0.35) and puromycin-containing media was added the next day to select for transductants. Selection was continued until 72 h post-transduction, which was considered the initial time point, t0. To identify IR sensitizers, the negative-selection screen was performed by subculturing at days 3 and 6 (t3 and t6), at which point the cultures were split into two populations. One was left untreated while the second was treated with 3 Gy of IR using a Faxitron X-ray cabinet (Faxitron, Tucson, AZ, USA) every 3 d after day 6. Cell pellets were frozen at day 18 for gDNA isolation. Screens were performed in technical duplicates and library coverage of ≥375 cells/sgRNA was maintained at every step. gDNA from cell pellets was isolated using the QIAamp Blood Maxi Kit (Qiagen) and genome-integrated sgRNA sequences were amplified by PCR using the KAPA HiFi HotStart ReadyMix (Kapa Biosystems, Wilmington, MA, USA). i5 and i7 multiplexing barcodes were added in a second round of PCR and final gel-purified products were sequenced on Illumina NextSeq500 systems to determine sgRNA representation in each sample. DrugZ40 was used to identify gene knockouts which were depleted from IR-treated t18 populations but not depleted from untreated cells.

Two-color competitive growth assay

20,000 cells were infected at an MOI of ~ 1.2 to ensure 100% transduction efficiency with either virus particles of NLS-mCherry LacZ-sgRNA or NLS-GFP GOI-sgRNA. 96 h following transduction, mCherry- and GFP-expressing cells were mixed 1:1 (2,500 cells + 2,500 cells) and plated with or without olaparib (16 nM) or etoposide (100 nM) in 12-well format. During the course of the experiment, cells were subcultured when near-confluency was reached. Olaparib- or etoposide-containing medium was replaced every three days. Cells were imaged for GFP- and mCherry signal the day of initial plating (t=0) and on days 3, 6, 9, 12, 15 and 18 (olaparib), or, in a separate set of experiments, on days 5, 10, 15 and 20 (etoposide). Cells were imaged using the automatic InCell Analyzer (GE Healthcare Life Sciences, Marlborough, MA, USA) with a 4x objective. Segmentation and counting of the number of GFP-positive and mCherry-positive cells was performed using an Acapella script (PerkinElmer, Waltham, MA, USA). Efficiency of indel formation was analysed by performing PCR amplification of the region surrounding the sgRNA sequence and TIDE analysis on DNA isolated from GFP-expressing cells 9 d post-transduction.

Mass spectrometry

Following 24 h of doxycycline-induction of stably integrated 293 FLP-IN cells (expressing Flag, Flag-FAM35A, Flag-REV7, Flag-C20orf196, Flag-CTC-534A2.2), cell pellets from two 150 mm plates were lysed in 50 mM HEPES-KOH (pH8.0), 100 mM KCl, 2 mM EDTA, 0.1% NP-40, 10% glycerol and affinity-purified using Flag-M2 magnetic beads (Sigma-Aldrich). Subsequently, digestion with trypsin (Worthington, Columbus, OH, USA) was performed on-beads. All immunoprecipitations were performed in biological replicates (three for CTC-534A2.2, five for C20orf196 and six for FAM35A and REV7).

For LC-MS/MS analysis, peptides were reconstituted in 5% formic acid and loaded onto a 12-15cm fused silica column with pulled tip packed with C18 reversed-phase material (Reprosil-Pur 120 C18-AQ, 3 μm, Dr. Maisch, Ammerbuch-Entringen, Germany). Peptides were analysed using an LTQ-Orbitrap Velos (Thermo Scientific) or a 6600 Triple TOF (AB SCIEX, Framingham, MA, USA) coupled to an Eksigent NanoLC-Ultra HPLC system and a nano-electrospray ion source (Proxeon Biosystems, Thermo Fisher Scientific). Peptides were eluted from the column using a 90-100 min gradient of acetonitrile in 0.1% formic acid. Tandem MS spectra were acquired in a data-dependent mode for the top 10 most abundant ions using collision-induced dissociation. After each run, the column was washed extensively to prevent carry-over.

Mass spectrometry data extraction and interaction scoring was performed essentially as described previously41. In short, raw mass spectrometry files were converted to mzXML and analyzed using the iProphet pipeline42, implemented within ProHits43. The data were searched against the human and adenovirus complements of the Uniprot (forward and reverse) database (Version 2017_09; reviewed Swiss-Prot entries only), to which common epitope tags were added as well as common contaminants (common contaminants are from the Max Planck Institute, http://141.61.102.106:8080/share.cgi?ssid=0f2gfuB, and the Global Proteome Machine, http://www.thegpm.org/crap/index.html; 85393 entries were searched). Mascot and Comet search engines were used with trypsin specificity (2 missed cleavages allowed) and deamidation (NQ) and methylation (M) as variable modifications. Charges +2, +3 and +4 were allowed with a parental mass tolerance of maximum 12 ppm and a fragment bin tolerance of 0.6 Da selected for Orbitrap instruments, while 35 ppm and 0.15 Da were allowed for the TripleTOF 6600. For subsequent SAINT analysis (see below), only proteins with an iProphet protein probability ≥ 0.95 were considered, corresponding to an estimated protein false discovery rate (FDR) of ~0.5%.

Interactions were analysed with SAINTexpress (v3.6.1)44,45. SAINT probability scores were computed independently for each replicate against eight biological replicate analyses of the negative control (FLAG alone; controls were “compressed” to six virtual controls to increase robustness as described46) and the average probability (AvgP) of the best three out of three (CTC534A2.2), five out of five (C20orf196) or six (FAM35A, REV7) biological replicates for each bait was reported as the final SAINT score. Preys with an estimated FDR ≤1% were considered true interactors (AvgP ≥0.91). The entire dataset, including the peptide identification and complete SAINTexpress output was deposited as a complete submission in ProteomeXchange through the partner MassIVE housed at the Center for Computational Mass Spectrometry at University of California, San Diego (UCSD; http://massive.ucsd.edu).

Data are available at MassIVE (ftp://massive.ucsd.edu/MSV000082207). Unique accession numbers are MSV000082207 and PXD009313, respectively. Data can also been viewed at the prohits website (prohits-web.lunenfeld.ca) under data set 29: Durocher lab. Data in Fig 1f is represented using Cytoscape, using analyses with an FDR ≤ 1 or 5 %.

Immunoprecipitation

1 x 10^7 293T cells were transfected with pcDNA5.1-FRT/TO -FLAG-c20orf196 (10 μg), -GFP-REV7 (2 μg), -V5-CTC534A2.2 (14 μg) and pGLUE-HA-Strep-FAM35A (14 μg) or empty vectors using a standard calcium phosphate or PEI protocol. After 48 h, cells were washed with PBS, scraped, and lysed in 1 ml of lysis buffer (50 mM Tris-HCl pH 8.0, 100 mM NaCl, 2 mM EDTA, 0.5% NP-40, 10mM NaF, 10 mM $MgCl_2$ and 10 U/ml Benzonase (Sigma-Aldrich)) on ice for 30 min. Lysates were centrifuged at 15,000g for 5 min at 4 °C, and supernatants were incubated with 100 μl of Streptavidin Sepharose High Performance beads (GE Healthcare) or Dynabeads M-280 Streptavidin magnetic beads (Invitrogen) for 1 h at 4 °C. Beads were washed 5 times with lysis buffer and eluted with 10 mM D-biotin (Invitrogen) in lysis buffer for 2 h at 4 °C. When applicable, the eluate was incubated with 20 μl of GFP-Trap_M resin (Chromotek, Planegg-Martinsried, Germany) for 1 h at 4 °C, washed 5 times with lysis buffer and eluted by boiling in sample buffer. Pull-downs and whole cell extracts were loaded onto SDS-PAGE gels, followed by immunoblotting and probing with indicated antibodies. For GFP-CTC534A2.2 immunoprecipitations, an identical GFP-Trap pulldown procedure as above was used. For V5-CTC534A2.2 immunoprecipitations, lysates from one confluent 10-cm dish of 293T cells transfected with 10 μg pcDNA5.1-FRT/TO-V5-CTC534A2.2 vector was incubated with 10 μg/ml anti-V5 antibody (Invitrogen) for 2 hours at 4 °C. Subsequently 50 μl of protein G Dynabeads (Invitrogen) was added to the lysates and incubated for an additional 1 h at 4 °C. Beads were washed 4 times with lysis buffer and boiled in 50 μl 2xSDS buffer.

Clonogenic survival assays

RPE1-hTERT *TP53*$^{-/-}$ cells were seeded in 10-cm dishes (WT: 250 cells: *BRCA1-KO 53BP1-KO*, 500 cells; *BRCA1-KO* or *BRCA1-KO C20orf196-KO*: 1,500 cells; *BRCA1-KO FAM35A-KO*: 750 cells) in the presence of 800 nM cisplatin or 16 nM olaparib or left untreated. Cisplatin dosing lasted 24 h, after which cells were grown in drug-free medium. Olaparib-containing medium was refreshed after 7 d. After 14 d, colonies were stained with crystal violet solution (0.4 % (w/v) crystal violet, 20% methanol) and manually counted. Relative survival was calculated for the drug treatments by setting the number of colonies in non-treated controls at 100%.

For *Rosa26*$^{CreERT2/wt}$ *Brca1*$^{SCo/\Delta}$ cells, Cre-mediated inactivation of the endogenous mouse *Brca1SCo* allele was achieved by overnight incubation of cells with 0.5 μM 4-hydroxytamoxifen (Sigma-Aldrich). Four days after switching, cells were seeded in triplicate at 10,000 cells per well in 6-well plates for clonogenic survival assays. For experiments with *Rosa26*$^{CreERT2/wt}$ *Brca1*$^{SCo/\Delta}$ p53-null cells, cells were plated in the presence of 15 nM olaparib. Cells were stained with 0.1% crystal violet one week later. Clonogenic survival assays with PARPi (olaparib) and ATMi (KU60019) combination treatment were performed as described previously with minor adjustments41. 5 x 10^3 KB1P-

G3 cells were seeded per well into 6-well plates on day 0, and then PARPi, ATMi, both or neither were added. The medium was refreshed every 3 d. On day 6, the ATMi alone and untreated groups were stopped and stained with 0.1% crystal violet, the other groups were stopped and stained on day 9. Plates were scanned with a GelCount (Oxford Optronics, Abingdon, UK). Quantifications were performed by solubilizing the retained crystal violet using 10% acetic acid and measuring the absorbance at 562 nm using a Tecan plate reader (Tecan, Männedorf, Switzerland).

Short term survival assays

10,000 RPE1-hTERT Cas9 *TP53*$^{-/-}$ parental cells and additional mutants (*BRCA1-KO* and/or *FAM35A-KO*) with or without stable integration of indicated eGFP-fusions by viral transduction were seeded in 12-well format with or without 200 nM olaparib (and 1 μg/mL doxycycline if applicable). Medium with olaparib (and doxycycline) was replaced after 4 d, and cells were trypsinized and counted after seven days using an automated Z2 Coulter Counter analyzer (Beckman Coulter, Indianapolis, IN, USA).

SUM149PT cells were plated at 500 cells per well in 384-well plates and varying amounts of talazoparib in DMSO were added the following day using an Echo 550 liquid handler (Labcyte, San Jose, CA, USA). After 5 d of growth, cell survival was assayed using CellTiter-Glo according to the manufacturer's protocol (Promega, Madison, WI, USA).

Immunofluorescence

For 53BP1 immunofluorescence (IF), cells were cultured on coverslips and treated with 5 or 10 Gy X-irradiation and fixed with 2-4% paraformaldehyde (PFA) 1 h after irradiation. Cells were permeabilized with 0.3% Triton X-100, followed by blocking in 10% goat serum, 0.5% saponin, 0.5% NP-40 in PBS (blocking buffer A). Cells were co-stained using 53BP1 and γH2AX primary antibodies (see Supplementary Table 7) in blocking buffer A for 1.5 h at room temperature, followed by 4 washes in PBS, incubation with appropriate secondary antibodies in blocking buffer A plus 0.8 μg/mL DAPI for 1.5 h at room temperature, and finally four washes in PBS.

For RAD51 IF, cells with or without stable integration of eGFP-tagged proteins or sgRNAs via viral transduction were grown on glass coverslips and treated with 10 Gy X-irradiation and recovered for 3 to 6 h (as indicated). Cells were fixated and extracted using 1% PFA, 0.5% Triton X-100 in PBS for 20 min at room temperature, followed by a second extraction/fixation using 1% PFA, 0.3% Triton X-100, 0.5% methanol in PBS for 20 min at room temperature. Blocking, primary and secondary antibody incubations (1.5 h at room temperature followed by 4 PBS washes) were performed in BTG buffer (10 mg/mL BSA, 0.5% Triton X-100, 3% goat serum, 1 mM EDTA in PBS) or PBS^{+} (0.5% BSA, 0.15% glycine in PBS).

For REV7 and RIF1 IF, cells were grown on glass coverslips, treated with 5 or 10 Gy X-irradiation and fixed with 2-4% PFA 1-2 h after irradiation. Cells were permeabilized with 0.3% Triton X-100. For REV7 blocking, primary and secondary antibody incubations (1.5 h at room temperature followed by 4 washes in PBS) were performed in blocking buffer A. For RIF1 blocking, primary and secondary antibody incubations (1.5 h at room temperature

followed by 4 washes) were performed in PBG buffer (0.2% cold water fish gelatin (Sigma Aldrich), 0.5% BSA in PBS).

For GFP-Shieldin focus and laser stripe analysis, U2OS or RPE1 cells were grown on glass coverslips and either transiently transfected with 1 μg vector expressing GFP-FAM35A or –CTC534A2.2, or virally transduced with GFP-FAM35A-expressing vector. 48 h post transfection, or 24 h post 0.5 μg/mL doxycyclin induction, cells were treated with 5 Gy X-irradiation or micro-irradiated, pre-extracted 10 min on ice with NuEx buffer (20 mM HEPES, pH 7.4, 20 mM NaCl, 5 mM MgCl2, 0.5% NP-40, 1 mM DTT and protease inhibitors) followed by 10 min 2% PFA fixation 1 h post-IR/micro-irradiation. Antibody staining and blocking were performed as described above except in PBS + 0.1% Tween-20 + 5% BSA using GFP and γH2AX antibodies.

0.8 μg/mL DAPI was included in all experiments to stain nuclear DNA. Coverslips were mounted using Prolong Gold mounting reagent (Invitrogen) or Aqua PolyMount (Polyscience, Warrington, PA, USA). Images were acquired using a Zeiss LSM780 laser-scanning microscope (Oberkochen, Germany), a Leica SP8 confocal microscope (Wetzlar, Germany) or a Zeiss AxioImager D2 widefield fluorescence microscope. Foci were manually counted.

RAD51 immunofluorescence in KB1P-G3 cells was performed as described previously, with minor modifications10. Cells were grown on 8-well chamber slides (Millipore). Ionizing-radiation induced foci were induced by γ-irradiation (10 Gy) 4 h prior to sample preparation. Cells were then washed in PBS++ (2% BSA, 0.15% glycine, 0.1% Triton X-100) and fixed with 2% PFA/PBS++ for 20 min on ice. Fixed cells were washed with PBS ++ and were permeabilized for 20 min in 0.2% Triton X-100/PBS++. All subsequent steps were performed in PBS++. Cells were washed thrice and blocked for 30 min at room temperature, incubated with the primary antibody for 2 h at RT, washed thrice and incubated with the secondary antibody for 1 h at room temperature. Lastly, cells were mounted and counterstained using Vectashield mounting medium with DAPI (H1500, Vector Laboratories, Burlingame, CA, USA).

Scale bars indicated in the figure panels represent 10 μm, unless stated otherwise.

LacR-RIF1N-terminus and FokI-induced focus formation

For monitoring recruitment of GFP-tagged Shieldin subunits to mCherry-LacR-Rif1(1-967) foci, 150,000 U2OS-FokI cells (known also as U2OS-DSB)47 were seeded on 6-well plates containing glass coverslips without any induction of FokI. 24 h after seeding, cells were transfected using 1μg of pDEST-mCherry-LacR or pDEST-mCherry-LacR-Rif1(1-967), if applicable, and 0.5-1 μg of GFP fusion expression vectors. Cells were fixed with 4% PFA 24-48 h after transfection. For monitoring the localization of the FAM35A N-terminus to Rif1(1-967) foci with siRNA knockdown of other Shieldin subunits, an essentially identical protocol was used with the following adjustments: 350,000 U2OS-FokI cells were reverse-transfected with Lipofectamine RNAiMAX-siRNA (10 nM) complex. 24 h after siRNA transfection, the mCherry-LacR and GFP fusion plasmids were transfected. Cells were fixed with 4% PFA 48 h after DNA transfection. For monitoring recruitment of GFP-tagged

Shieldin subunits to DSBs at the LacO array, FokI stabilization and nuclear translocation was induced by treating cells with 0.1 μM Shield1 (Clontech, Mountain View, CA, USA) and 10 μg/mL hydroxytamoxifen for 4 h.

ImageJ (https://imagej.nih.gov/ij/) was used to quantify foci in the U2OS-FokI system. An mCherry focus and DAPI nuclear signal were used to generate masks. The average GFP fluorescence or immunofluorescence intensity in the mCherry focus mask was divided by the corresponding average nuclear intensity, and the ratio is reported. Cells displaying a ratio of focus/nuclear average intensity >3 are defined as containing a focus.

Microirradiation

For laser microirradiation, virally transduced RPE1 cells expressing the indicated eGFP-tagged proteins were grown on glass coverslips and transfected with siRNAs. 48 h post-transfection, protein expression was induced using 0.5 μg/mL doxycycline, and 24 h later cells were presensitized with 1 μg/mL Hoechst for 15 min at 37 °C. DNA damage was introduced with a 355 nm laser (Coherent, Santa Clara, CA, USA, 40mW) focused through a Plan-Apochromat 40x oil objective to yield a spot size of 0.5-1 mm using a LSM780 confocal microscope (Zeiss) and the following laser settings: 100% power, 1 iteration, frame size 128 x 128, line step 7, pixel dwell: 25.21 μs.

Traffic light reporter assay

Cells were infected with pCVL.TrafficLightReporter.Ef1a.Puro lentivirus at a low MOI (0.3-0.5) and selected with puromycin (15 μg/μl). 7 x 10^5 cells were nucleofected with 5 μg of pCVL.SFFV.d14GFP.Ef1a.HA.NLS.Sce(opt).T2A.TagBFP plasmid DNA in 100 μL of electroporation buffer (25 mM Na_2HPO_4 pH 7.75, 2.5 mM KCl, 11 mM $MgCl_2$), using program T23 on a Nucleofector 2b (Lonza). After 72 h, GFP and mCherry fluorescence was assessed in BFP-positive cells using a Fortessa X-20 (BD Biosciences, San Jose, CA, USA) flow cytometer.

Phospho-RPA immunoblotting

For phospho-RPA staining, CH12 cells were left untreated, or were treated with 25 Gy of ionizing radiation using a Faxitron X-ray cabinet, and were then collected by centrifugation 3 h later. Pellets were lysed on ice for 10 min in high salt lysis buffer (50 mM Tris-HCl pH 7.6, 300 mM NaCl, 1 mM EDTA, 1% Triton X-100, 1 mM DTT, 1x EDTA-free protease inhibitor cocktail (Roche, Basel, Switerzerland)), cleared by centrifugation at 20,000 x *g* for 10 min at 4 °C, and quantified by bicinchoninic acid assay (BCA; Pierce, Thermo Fisher Scientific). Equal amounts of whole-cell extracts were separated by SDS-PAGE on 4-12% Bis-Tris gradient gels (Invitrogen), transferred to nitrocellulose and immunoblotted for pRPA32 (S4/S8).

Mouse mammary tumour models

All animal experiments were approved by the Animal Ethics Committee of The Netherlands Cancer Institute (Amsterdam, the Netherlands) and performed in accordance with the Dutch Act on Animal Experimentation (November 2014). KB1P4 tumor organoids were transduced using spinoculation as described previously48. NMRI-nude female mice were

purchased from Janvier Laboratories and used for transplantation studies at the age of 6-9 weeks. A power analysis was performed to calculate that a minimum of 8 mice per group were needed to achieve a power of 0.8 (two-sided test, alpha=0.05).Tumor organoids were allografted in mice as described previously with minor adjustments35. Briefly, tumor organoids were collected, incubated with TripLE at 37 °C for 5 min, dissociated into single cells, washed and embedded in a 1:1 mixture of tumor organoid culture medium and Basement Membrane Extract (Trevigen) in a cell concentration of 10^4 cells per 40 μL. Subsequently, 10^4 cells were injected in the fourth right mammary fat pad of NMRI nude mice. Mammary tumor size was determined by caliper measurements and tumor volume was calculated (0.5 x length x $width^2$). Treatment of tumor-bearing mice was initiated when tumors reached a size of 50-100 mm^3. Mice were randomly allocated into the untreated (n = 8) or olaparib treatment group (n = 8). Olaparib was administered in a blinded fashion at 100 mg/kg intraperitoneally for 80 consecutive days. Animals were sacrificed with CO_2 when the tumor reached a volume of 1,500 mm^3. The tumor was collected, fixed in formalin for histology and several tumor pieces were harvested for DNA analysis.

Class switch recombination assays

To induce switching in CH12F3-2 murine B cell lymphoma cells, $2x10^5$ cells were cultured in CH12 media supplemented with a mixture of IL4 (10 ng/mL, R&D Systems #404-ML-050, Minneapolis, MN, USA), TGFβ (1 ng/mL, R&D Systems #7666-MB-005) and anti-CD40 antibody (1 μg/mL, #16-0401-86, eBioscience, Thermo Fisher) for 48 h. Cells were then stained with anti-IgA-PE and fluorescence signal was acquired on an LSR II or Fortessa X-20 flow cytometer (BD Biosciences). To probe AID levels in the stimulated cells, immunoblotting was performed on total cell lysates using anti-AID and anti-β-actin antibodies (Supplementary Table 7). Band quantification was analysed by ImageJ.

Plasmid integration assay

200,000 RPE1 cells were seeded into 6-well plates and 24 h later transfected with 2 μg of *Bam*HI/*Eco*RI-linearized peGFP-c1 using PEI. 72 h post-transfection, cells were seeded for colony formation into 10 cm dishes in the presence (50,000 cells per dish) or absence (500 cells per dish) of 600 μg/mL G418. At this point, transfection efficiency was analysed by measuring GFP-positivity using flow cytometry. Medium with G418 was refreshed every 3 d. 14 d after seeding, colonies were stained with crystal violet solution and manually counted. NHEJ efficiency was calculated according to the following formula:

$$\frac{\%\ \text{surviving colonies on selection}}{(\%\ \text{of surviving colonies without selection}) \times (\%\ \text{of transfected cells})}$$

The data shown for the different KO clones in ED Fig 8e is representing NHEJ efficiency as calculated with the above formula, followed by normalisation to WT cells (for which NHEJ efficiency is set to 100%).

DNA binding assays

Shieldin proteins were isolated using the immunoprecipitation protocol described above with the following modifications. 293T cells were transfected with pGLUE- FAM35A(421-904),

the indicated mutants of this construct, or the empty pGLUE Strep/HA-tagging vector and pcDNA5.1-FRT/TO -FLAG-C20orf196 in a 2:1 ratio for a total of 10 μg per 10 cm dish. Complexes were immunoprecipitated as described, except using a reduced NP-40 detergent concentration (0.1%) for the last two washes and elution buffer. Eluted proteins were concentrated using Amicon Ultra 0.5 ml 10K centrifugal filter units (Millipore). Concentrations of isolated proteins were estimated by SDS-PAGE and Coomassie staining, followed by comparison to a standard curve of known bovine serum albumin (BSA) concentrations measured by fluorescence in the 700 nM channel of the Odyssey imager (LI-COR). A radiolabeled ssDNA probe was prepared by T4 polynucleotide kinase (New England Biolabs, Ipswich, MA, US) phosphorylation of HPLC-purified 59-nt DNA oligo (BioBasic, Markham, ON, CA; TACGTTAGTATGCGTTCTTCCTTCCAGAGGTTTTTTTTTTTTTTTTTTTTTTTTTT) using [γ-32P]-ATP (3000 Ci/mmol, 10 mCi/ml; Perkin-Elmer, Woodbridge, ON, CA). Unlabeled competitors were prepared using the same oligo sequence alone or hybridized to the complementary sequence (AAAAAAAAAAAAAAAAAAAAAAAAAAAAAACCTCTGGAAGGAAGAACGCATACTAACGTA) by heating at 80 °C for 10 mins and gradual cooling to room temperature overnight.

For electrophoretic mobility shift assays, 20 nM of labeled ssDNA probe was incubated with purified proteins for 20 min in the elution buffer with the addition of 1 mM DTT and 1 mg/ml BSA at room temperature. Glycerol was then added to a final concentration of 8.3% and resolved on 6% acrylamide-TAE gels. Gels were adhered onto blotting paper (VWR) and enclosed in plastic wrap. Gels were exposed to a storage phosphor screen (GE Healthcare) and visualized using a Typhoon FLA 9500 biomolecular imager (GE Healthcare). Dissociation constant (K_D) was determined in GraphPad Prism from nonlinear regression analysis assuming single-site specific binding of saturation titration experiments, defining all signal above the free probe band to be bound probe, as measured in ImageQuant TL(GE Healthcare). The fraction of probe bound is defined as:

$$\frac{\text{signal of bound probe}}{\text{signal of bound probe}+\text{signal of free probe}}$$

and the concentration of unbound FAM35AC-C20orf196 (referred in the text as SHLD2C-SHLD1) complex is calculated by:

$$\text{Initial concentration of SHLD2CSHLD1} - \text{Fraction of probe bound} * \text{Initial concentration of ssDNA probe}$$

given the assumption of 1:1 binding.

Statistical analysis

All data is represented as individual replicates and replicate number, mean and error bars are explained in the figure legends. Used statistical tests (all common tests) and resulting p-values are indicated in the figure legends and/or figure panels and have been generated using GraphPad Prism software.

Europe PMC Funders Author Manuscripts

Data availability statement

All source data represented in the graphs displayed in this article are available online (Supplementary Data files 1-12). Uncropped Western blots can be found online as Supplementary Figure 1. Data of the CRISPR Cas9 screens are included as Supplementary Table 1 (PARPi positive selection screens) or Supplementary Table 4 (IR sensitivity dropout screen). IP-MS data (Supplementary Table 3) are available at MassIVE (ftp://massive.ucsd.edu/MSV000082207, with unique accession numbers MSV000082207 and PXD009313). IP-MS data can also been viewed at the prohits website (prohits-web.lunenfeld.ca) under data set 29: Durocher lab.

Extended Data

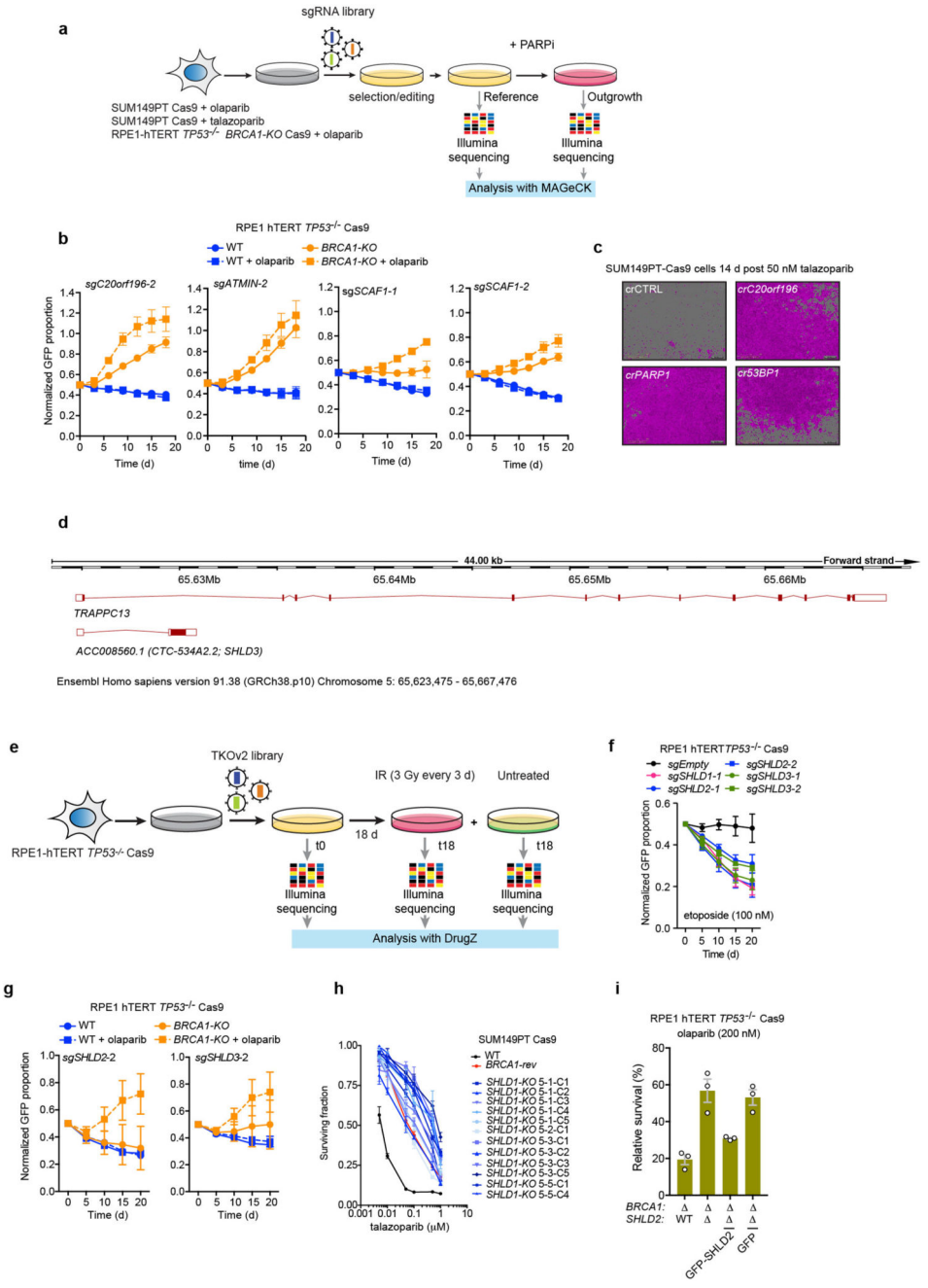

ED Figure 1. Supporting data for the identification of the Shieldin complex and its role in the response to genotoxic treatments.

a, Schematic of the PARPi resistance screens. **b,** Competitive growth assays determining the capacity of the indicated sgRNAs to cause resistance to PARP inhibitors in RPE1 *BRCA1-KO* cells. Data is presented as the mean fraction of GFP-positive cells ± SEM, normalized to day 0 (n = 3, independent viral transductions). Gene editing efficiencies of the sgRNAs can be found in Supplementary Table 2. Note that we have not been able to obtain TIDE data for

Europe PMC Funders Author Manuscripts

the *ATMIN*-targeting sgRNAs. **c,** Representative images of SUM149PT-Cas9 cells transfected with indicated crRNAs (see Methods) and exposed to 50 nM talazoparib for 14 d. Purple coloration indicates cells detected by Incucyte live-cell imaging. Scale bar represents 100 μm. The data is a representative set of images from two biologically independent experiments. **d,** Screenshot of the genomic locus surrounding human CTC-534A2.2 taken from ENSEMBL. **e,** Schematic of the screen performed in RPE1-hTERT *TP53*$^{-/-}$ cells stably expressing Cas9 to study genes mediating IR-sensitivity. **f-g,** Competitive growth assays measuring the capacity of the indicated sgRNAs to cause resistance to etoposide (100 nM) in RPE1 WT cells (f) or PARP inhibitors (16 nM) in RPE1 *BRCA1-KO* cells (g). Data is presented as the mean fraction of GFP-positive cells ± SD, normalized to day 0 (n = 3, independent viral transductions). Gene editing efficiencies of the sgRNAs can be found in Supplementary Table 2. **h,** Talazoparib sensitivity in 11 *SHLD1-KO* SUM149PT clones obtained after co-transfection of tracrRNA and one of four distinct *SHLD1* crRNAs (5-1, 5-2, 5-3 or 5-5). Each clone was exposed to talazoparib in a 384-well plate format for five days. As a comparison, talazoparib sensitivity in parental SUM149PT cells with WT SHLD1 (WT) is shown, as is talazoparib resistance in a *BRCA1* revertant subclone (*BRCA1-rev)* of SUM149PT49. Bars represent the mean ± SD (n=4 biologically independent experiments). ANOVA was performed for each *SHLD1*-KO clone vs. WT using Dunnett correction for multiple comparisons, $p<10^{-15}$. Gene editing efficiencies can be found in Supplementary Table 2. **i,** *BRCA1-KO* and *BRCA1-KO/SHLD2-KO* cells were virally transduced with expression vectors for GFP alone or GFP-SHLD2. Sensitivity to olaparib (200 nM) was determined by a short-term survival assay in the presence of 1 μg/mL doxycycline to induce protein expression. Data is represented as dots for every individual experiment with the bar representing the mean ± SD (n=3).

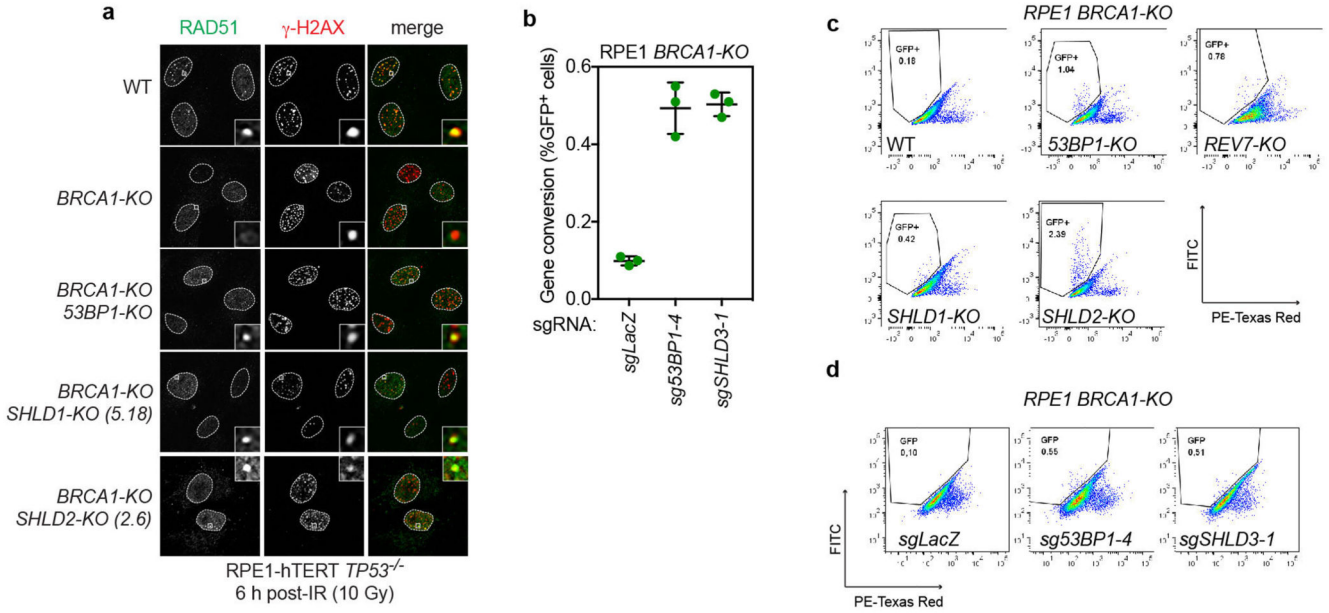

ED Figure 2. Supporting data that Shieldin inhibits HR.

a, Representative micrographs of RAD51 focus formation in the indicated RPE1 cell lines (data quantitated in Fig 2d, n ≥ 3). **b,** Traffic light reporter (TLR) assay testing RPE1 *BRCA-KO* cells virally transduced with sgRNAs targeting *53BP1* or *SHLD3*. Data is represented as dots for individual experiments with the bar representing the mean ± SD (n=3). Gene editing efficiencies of the sgRNAs can be found in Supplementary Table 2). **c,** Representative flow cytometry plots of cells analysed with the TLR assay (data quantitated in Fig 2e, n ≥ 3). **d,** Representative flow cytometry plots of cells analysed with the TLR assay (data quantitated in ED Fig 2b).

Europe PMC Funders Author Manuscripts

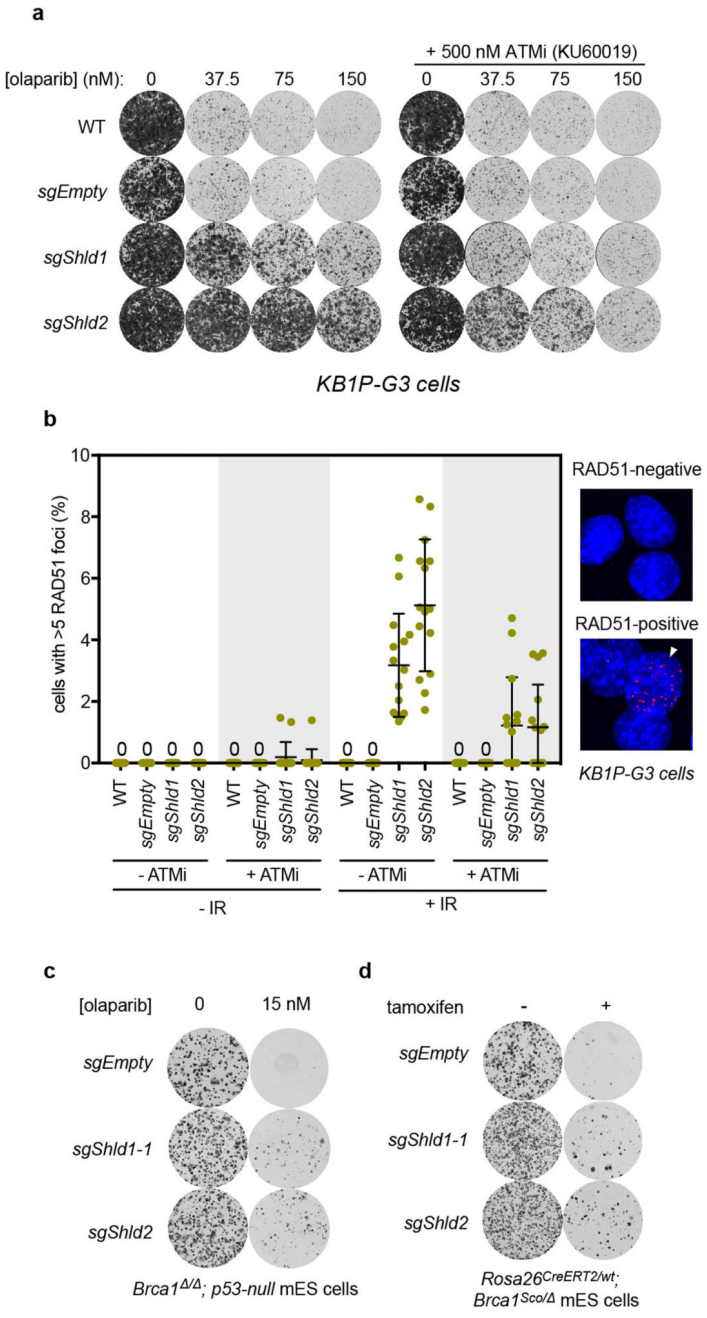

ED Figure 3. Supporting data that mouse Shieldin promotes resistance to PARP inhibition in *Brca1*-mutated cells and tumours.

a, Clonogenic survival assays of transduced KB1P-G3 cells treated with indicated olaparib doses ± ATM inhibitor (ATMi) KU60019 (500 nM). On day 6, the ATMi alone and untreated groups were stopped and stained with 0.1% crystal violet; the other groups were stopped and stained on day 9. Data shown is a representative set from 3 biologically independent experiments (with 3 technical replicates each). **b,** Left, quantitation of Rad51 focus formation in parental KB1P-G3 (*Brca1*$^{-/-}$; *Trp53*$^{-/-}$) cells or KB1P-G3 cells that were

Europe PMC Funders Author Manuscripts

transduced with the indicated lentiviral sgRNA vectors. Cells were fixed without treatment or 4 h after irradiation (10 Gy dose). Each data point represents a microscopy field containing a minimum of 50 cells; the bar represents the mean ± SD (n=15). Right, representative micrographs of Rad51-negative and -positive cells (the latter is indicated by an arrowhead). DNA was stained with DAPI. **c**, Clonogenic survival assay of *Rosa26*$^{CreERT2/wt}$*; Brca1*$^{\Delta/\Delta}$*; p53-null* mES-cells virally transduced with the indicated sgRNA and treated without or with 15 nM olaparib for 7 d. Gene editing efficiencies of the sgRNAs can be found in Supplementary Table 2. Data shown is a representative set from 3 biologically independent experiments (with ≥ 2 technical replicates each). **d,** Clonogenic survival assay of *Rosa26*$^{CreERT2/wt}$*;Brca1*$^{Sco/\Delta}$ mES-cells virally transduced with the indicated sgRNA and treated without or with 0.5 μM tamoxifen to induce BRCA1 depletion. Gene editing efficiencies of the sgRNAs can be found in Supplementary Table 2. Data shown is a representative set from 2 biologically independent experiments (with 3 technical replicates each).

Europe PMC Funders Author Manuscripts

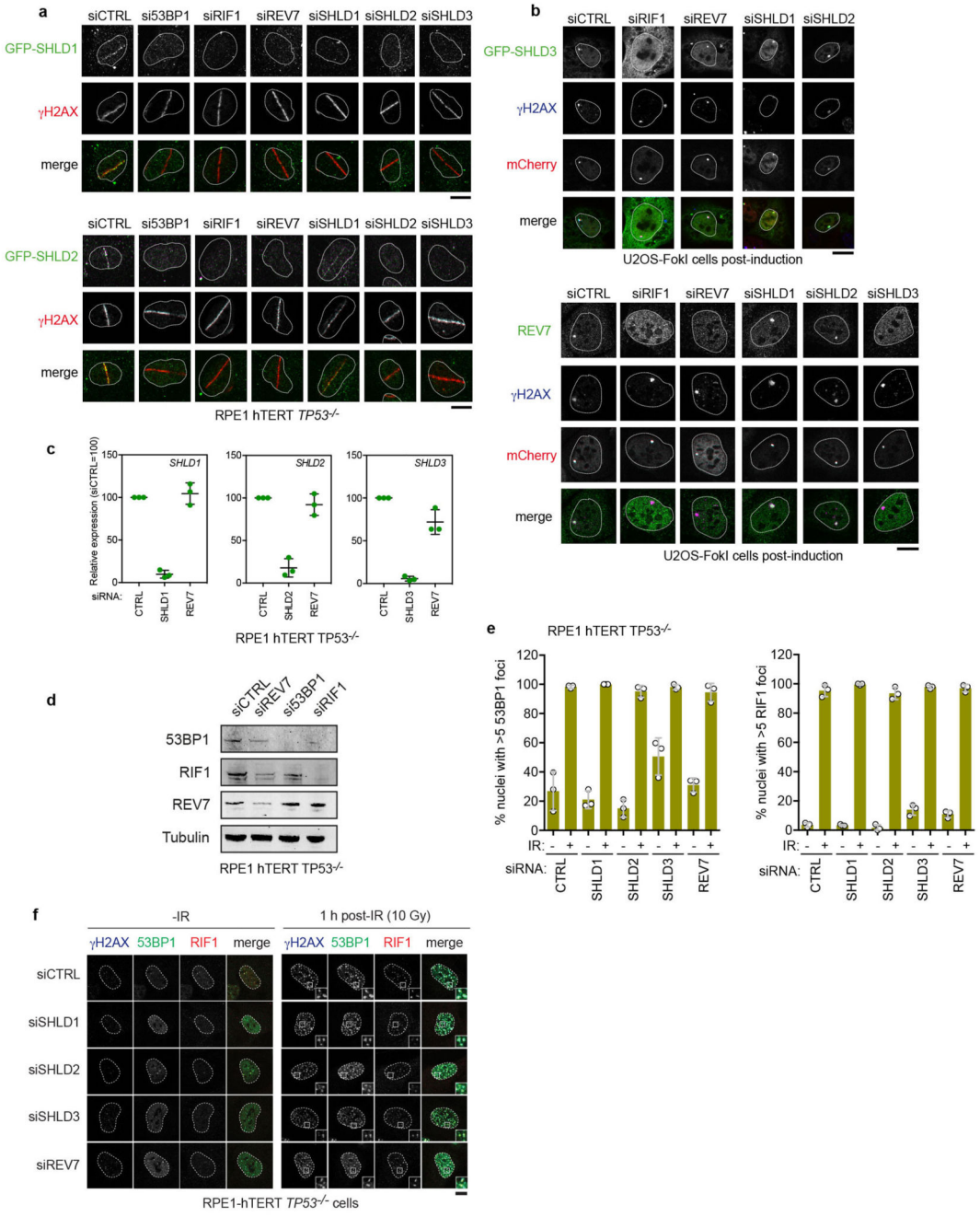

ED Figure 4. Supporting data that Shieldin localizes to DSB sites

a, Representative micrographs of the experiments quantitated in Fig 3c. **b,** Representative micrographs of the experiments quantitated in Fig 3e. **c,** Quantitation of mRNAs for *SHLD1, SHLD2* and *SHLD3*. RPE1 cells were transfected with siCTRL (non-targeting control siRNA) or siRNA targeting the indicated Shieldin subunits. 48 h post-transfection, mRNA was purified and reverse transcribed before being assayed by quantitative real-time PCR. Data were normalized to the amount of *GAPDH* mRNA and expressed relative to the corresponding value for cells transfected with siCTRL. Data is presented as the mean ± SD

(n=3, independent siRNA transfections). **d,** Whole cell extracts from RPE1 WT cells transfected with the indicated siRNAs were processed for immunoblotting with the indicated antibodies. Tubulin is used as a loading control (n=1 experiment; siRNA efficiency is also monitored by immunofluorescence). **e,** Quantitation of 53BP1 and RIF1 recruitment to IR-induced DSBs (1 h post-irradiation with 10 Gy) following depletion of the indicated Shieldin components. Data is represented as the mean ± SD (n=3, independent siRNA transfections). **f,** Representative micrographs of the experiments quantitated in ED Fig 4e.

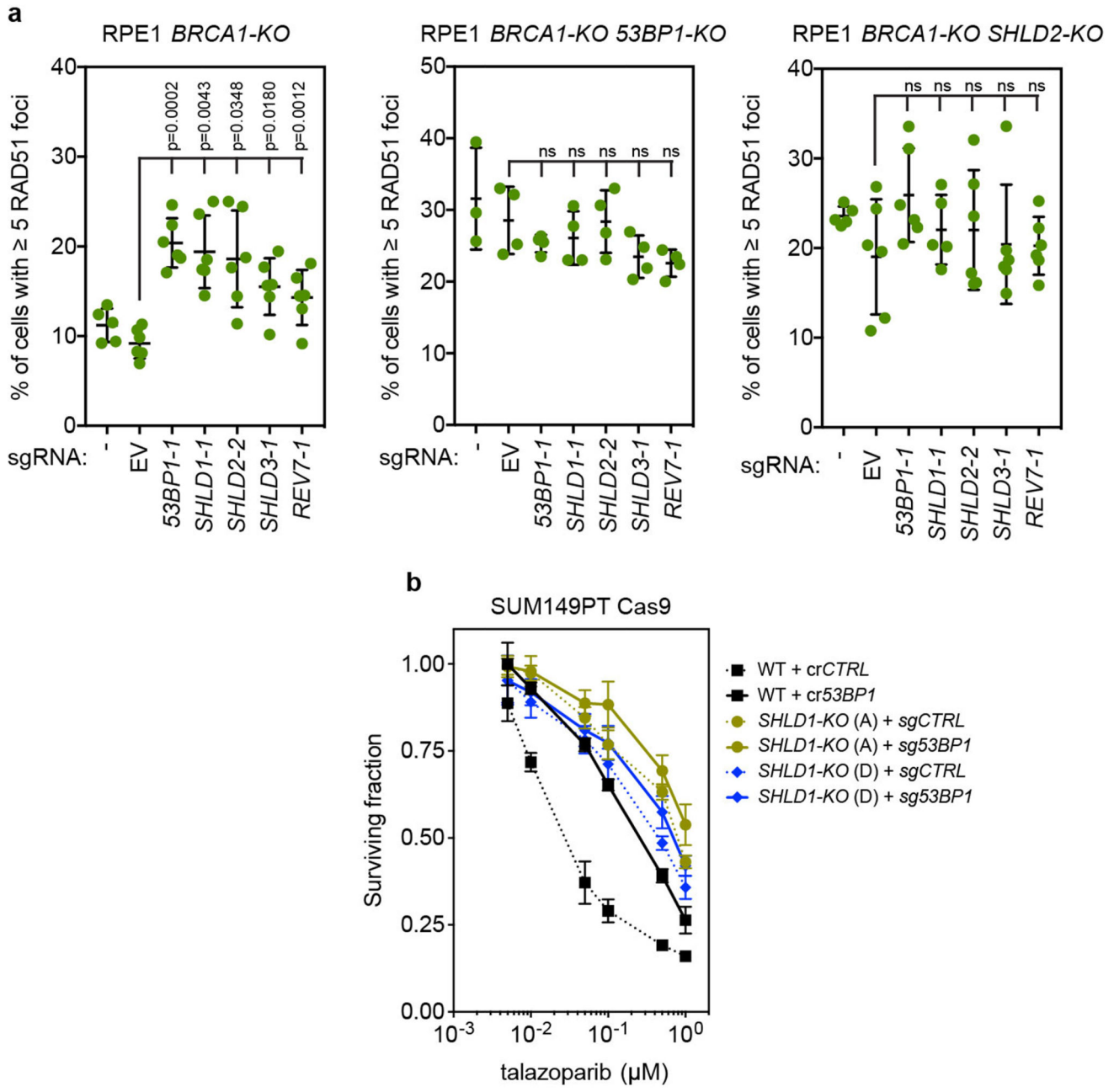

ED Figure 5. Data supporting epistasis between 53BP1 and Shieldin factors.

Europe PMC Funders Author Manuscripts

a, Quantitation of RAD51 focus formation 3 h post-irradiation (10 Gy) in RPE1 *BRCA1-KO* (left panel), *BRCA1-KO/53BP1-KO* (middle panel) and *BRCA1-KO/SHLD2-KO* (right panel) cells after viral transduction with the indicated sgRNAs (editing efficiency can be found in Supplementary Table 2) or empty vector (EV). Data is represented as the mean ± SD (for *BRCA1-KO 53BP1-KO*, n=4 biologically independent IF experiments; for *BRCA1-KO* and *BRCA1-KO SHLD2-KO*, n=6 biologically independent IF experiments). P-values were calculated using a two tailed unpaired t-test. Left panel: BRCA1-KO EV vs sg*53BP1-1* p=0.0002; EV vs sg*SHLD1-1* p=0.0043; EV vs sg*SHLD2-2* p=0.0348; EV vs sg*SHLD3-1* p=0.0180; EV vs sg*REV7-1* p=0.0012). Middle and right panel: all comparisons to the EV condition were non-significant (ns). Values for *BRCA1-KO 53BP1-KO* EV vs sg*53BP1-1* p=0.2332; EV vs sg*SHLD1-1* p=0.4451; EV vs sg*SHLD2-2* p=0.9632; EV vs sg*SHLD3-1* p=0.1187; EV vs sg*REV7-1* p=0.0568. Values for *BRCA1-KO SHLD2-KO*: EV vs sg*53BP1-1* p=0.0550; EV vs sg*SHLD1-1* p=0.1864; EV vs sg*SHLD2-2* p=0.3568; EV vs sg*SHLD3-1* p=0.4641; EV vs sg*REV7-1* p=0.2888. **b,** Talazoparib sensitivity of WT or two independent *SHLD1-KO* SUM149PT-dox-Cas9 clones (A and D) virally transduced with an sgRNA targeting *53BP1* (*sg53BP1*) or a control non-targeting sgRNA (*sgCTRL*), following induction of Cas9. Data is presented as the mean ± SD (n=3 biologically independent experiments).

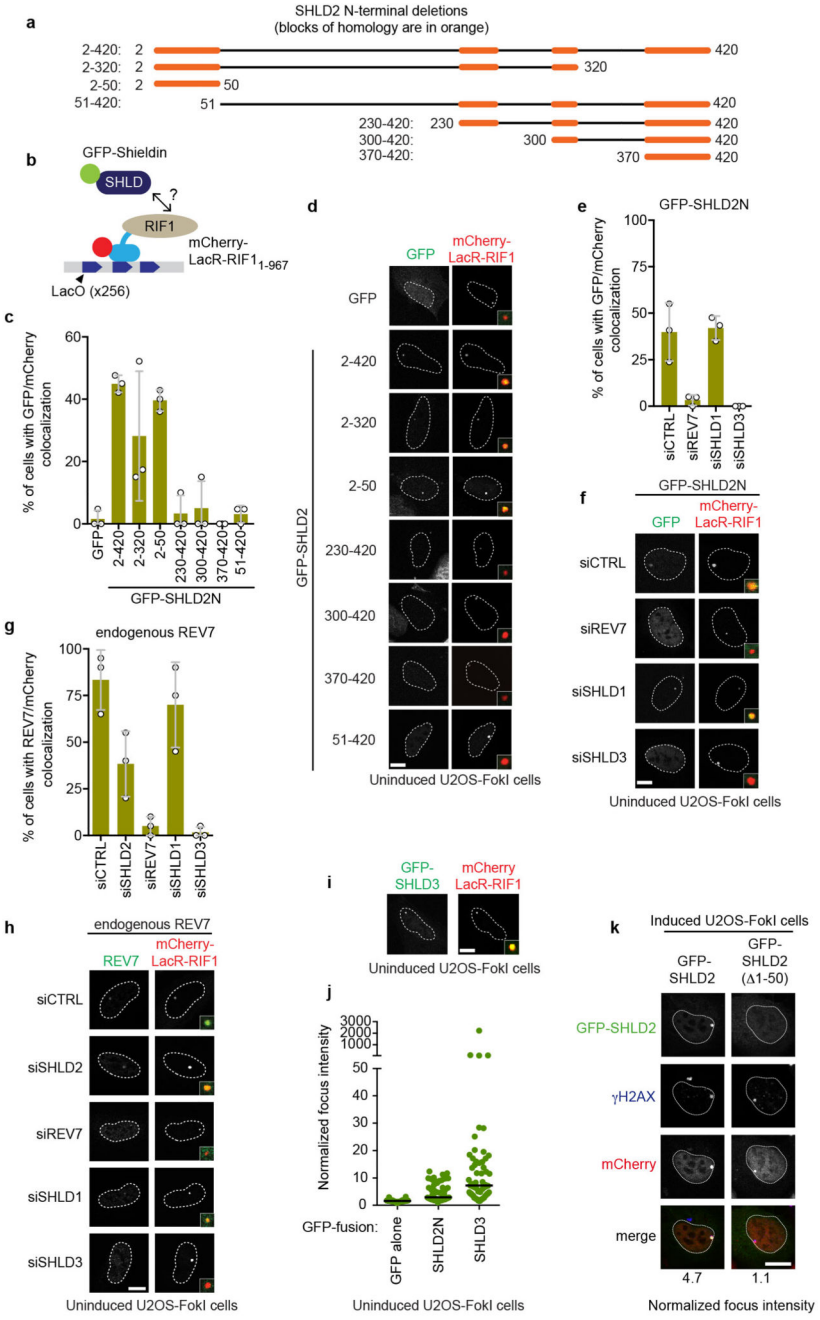

ED Figure 6. Data supporting the co-localization of Shieldin with RIF1 on chromatin.

a, Representation of the deletion mutants of SHLD2N used in ED Fig 6cd. The orange shading indicates blocks of homology. **b,** Schematic of the LacR-RIF1 chromatin recruitment assay. **c,** Quantitation of the experiment shown in ED Fig 6d. Colocalization was considered positive when the average GFP intensity at the mCherry focus was 3-fold over background nuclear intensity. A minimum of 20 cells were imaged per biological replicate (circles); the bar represents the mean ± SD (n=3). **d,** Representative images of the data quantitated in ED Fig 6c. The main focus is shown in inset and the scale bar = 10 μm. **e-h,**

Europe PMC Funders Author Manuscripts

Quantitation (e,g) and representative micrographs (f,h) of overexpressed GFP-SHLD2N and mCherry-LacR-RIF1(1-967) co-transfected into uninduced U2OS-FokI cells along with siRNA against Shieldin complex subunits after processing for mCherry and GFP (e,f) or mCherry and REV7 (g,h) immunofluorescence. Colocalization was considered positive when the average GFP or REV7 intensity at the mCherry focus was 3-fold over background nuclear intensity. A minimum of 20 cells were imaged per condition (circles); the bar represents the mean ± SD (n=3 biologically independent experiments). **i,** Representative images of the data quantitated in ED Fig 6j. The main focus is shown in inset and the scale bar = 10 μm. **j,** Quantitation of GFP intensity at the mCherry-LacR-RIF1(1-967) focus, normalized to nuclear background. Each data point represents a cell transfected with the vector coding for the indicated GFP fusion. The line is at the median. The data is an aggregate of three independent experiments with a minimum of 20 cells counted (total cells counted: 62, 60, and 61 for GFP, GFP-SHLD2C, and GFP-SHLD3, respectively). **k,** mCherry-LacR-FokI colocalization with full length or N-terminally truncated (Δ1-50) GFP-SHLD2. Mean normalized focus intensity is shown from a total of 59 (SHLD2 full length) or 56 (SHLD2 Δ1-50) cells counted (n=2 biologically independent experiments).

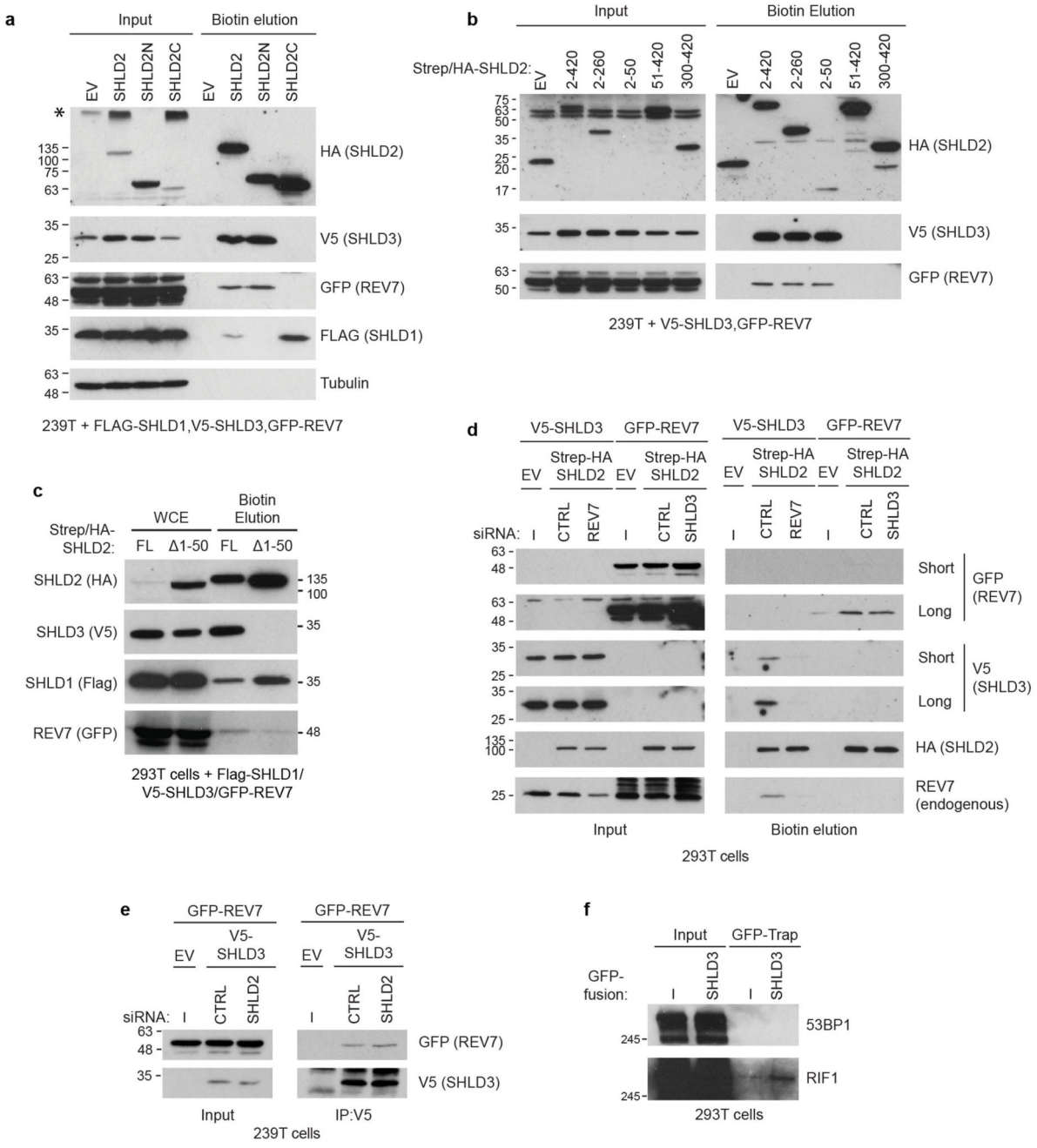

ED Figure 7. Mapping the architecture of the Shieldin complex.

a, Streptavidin pulldown analysis determining which region of SHLD2 associates with the other Shieldin subunits. Whole cell extracts (WCEs) of 293T cells transfected with an expression vector for FLAG-SHLD1, V5-SHLD3, GFP-REV7 and Strep/HA-tagged SHLD2, SHLD2N (residues 2-420), SHLD2C (residues 421-904), or empty Strep/HA vector (EV) were incubated with streptavidin resin and bound proteins were eluted with biotin. WCEs and elutions were analysed by SDS-PAGE and immunoblotting with the indicated antibodies. Tubulin was used as a loading control. Results are representative set of

Europe PMC Funders Author Manuscripts

immunoblots from 2 independent experiments. * denotes a non-specific band. **b,** Mapping the SHLD3 and REV7 binding sites on the SHLD2 N-terminus through streptavidin pulldowns with different SHLD2 constructs (detailed in ED Fig 6a) and immunoblotting. Results are a representative of a set of immunoblots from 3 independent experiments. **c,** Affinity purification of Shieldin complex components using N-terminally truncated SHLD2(Δ1-50) analyzed by immunoblotting (representative of three independent experiments). **d,** Streptavidin pulldown analysis of SHLD2 association with REV7 and SHLD3. 293T cells were transfected with siRNAs and expression vectors for epitope-tagged Shieldin components as indicated (EV, empty Strep/HA vector). WCEs were incubated with streptavidin resin and bound proteins were eluted with biotin. WCEs and elutions were analysed by SDS-PAGE and immunoblotted with the indicated antibodies. Short and long exposures are shown for GFP and V5 immunoblots (n=1). **e,** Dependency of V5-SHLD3 co-immunoprecipitation with GFP-REV7. 293T cells were transfected with siRNAs and expression vectors for epitope-tagged REV7 and SHLD3 as indicated (EV, empty V5 vector). WCEs were incubated with anti-V5 antibody and protein G resin. Bound proteins were boiled in SDS sample buffer and analysed by immunoblotting with GFP and V5 antibodies (n=1). **f,** Association between SHLD3 and RIF1. WCEs of 293T cells transfected with an expression vector for unfused GFP (-) or GFP-SHLD3 (SHLD3) were incubated with GFP-Trap resin. Bound proteins were boiled in SDS sample buffer and analysed by SDS-PAGE and immunoblotting against 53BP1 and RIF1. Results are representative of 2 SHLD3 IPs, utilizing SHLD3 fused to GFP (shown here) and V5 (show in Fig 3g) affinity tags.

Europe PMC Funders Author Manuscripts

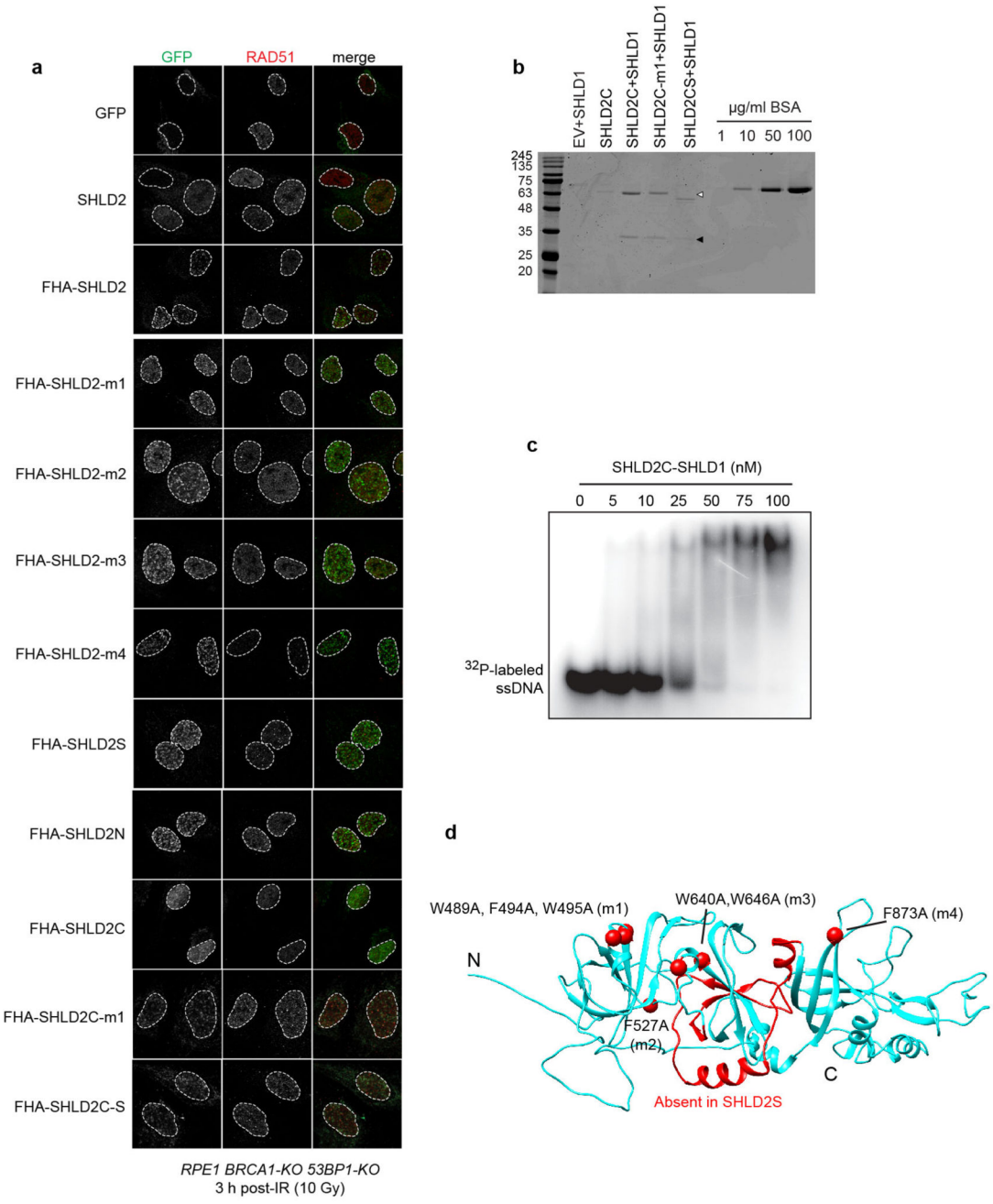

ED Figure 8. Controls supporting the role of Shieldin in promoting physiological NHEJ.

a, Representative dot plots of the flow cytometry data obtained (of n=3 biologically independent experiments) to assess class switching in Fig 3h. CSR was determined as the percentage of IgA^+ cells following stimulation after subtracting the baseline percentage of IgA^+ cells in the indicated clones (values in brackets). **b, c,** Epistasis analysis of Shieldin and 53BP1 in CSR. Shown is the percentage of class switching in CH12F3-2 wild type, single knockout, or double knockout cells (as indicated) following stimulation. Each data point represents a biological replicate; the line represents the mean ± SD (n=3). Genomic

editing efficiencies of the sgRNAs can be found in Supplementary Table 2. **d,** Whole cell extracts of the indicated CH12F2-3 clones were probed for AID and β-actin (loading control) by immunoblotting and were quantitated by densitometry. Each data point represents a biological replicate; the line represents the mean ± SD (n=9 for WT, n=3 for other samples). **e,** Random plasmid integration of linearized pcGFP-c1 conferring G418 resistance. Resistant colonies were quantified after 14 d. Bar represents the mean ± SD with WT cells set at 100% (left panel: n=5, right panel n=4 except SHLD2-KO (2.7) n=3 biologically independent experiments). **f,** Representative images of the plasmid integration assays quantitated in ED Fig 3e. **g,** Unirradiated CH12F3-2 clones (25 Gy) were immunoblotted for RPA2 phosphorylation (a representative set from n=3 biological replicates; data relates to Fig 3i).

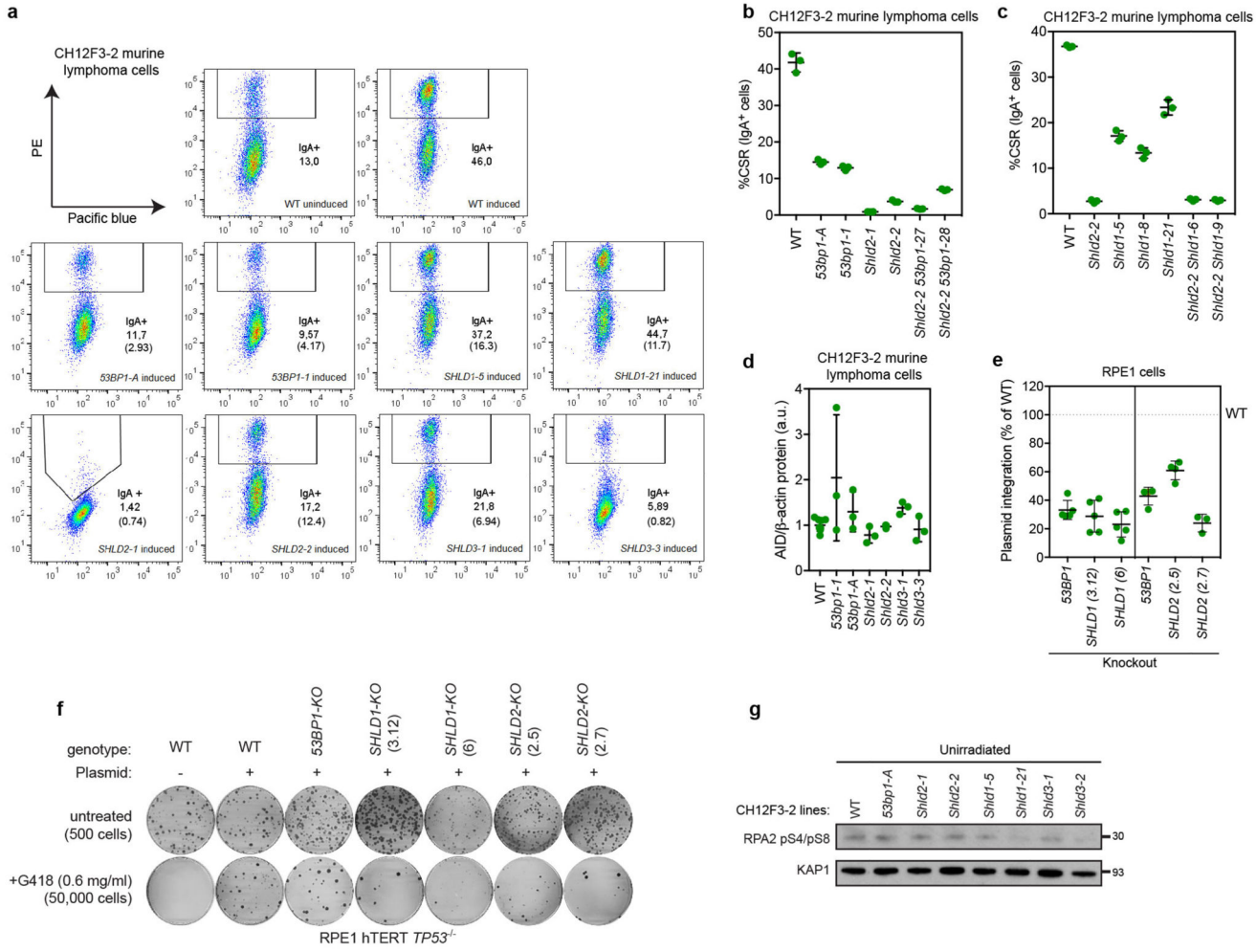

ED Figure 9. Data supporting the role of DSB-targeted SHLD2 in the suppression of HR and the mapping of the SHLD2C-SHLD1 complex binding to ssDNA.

a, Representative micrographs of RPE1 *BRCA1-KO/53BP1-KO* cells transduced with the indicated GFP-fusion proteins, pre-extracted, fixed and stained for RAD51 and GFP 3 h post-IR (10 Gy). Protein expression was induced for 24 h before IR using 1 μg/mL

doxycycline. Data relates to Fig 4b. Note that due to the pre-extraction required for visualization of RAD51 foci, the visualization of non-FHA tagged SHLD2 is lost. **b,** SDS-PAGE analysis of purified SHLD2C-SHLD1 complexes. Strep/HA-SHLD2(421-904)–Flag-SHLD1 complexes were purified from transiently transfected 293T cells. Concentrations of purified proteins were estimated by Coomassie staining and comparison to a standard curve of known BSA concentrations visualized by fluorescence at 700 nm. SHLD2C-m1 and SHLD2CS denote SHLD2C constructs carrying the OB fold m1 mutation and the internal deletion (Δ655-723) corresponding to the naturally occurring splice variant of SHLD2, respectively. Open and filled arrowheads mark the bands corresponding to SHLD2C and SHLD1, respectively. EV refers to empty Strep/HA vector. Shown is a representative stained gel from 2 independent experiments. **c,** Representative image of the [^{32}P]-labeled ssDNA EMSA with SHLD2C-SHLD1 for K_D determination shown in Fig 4e. **d**, Model of the SHLD2-OB fold domains and the engineered mutations (red spheres, point mutations; red ribbons, splice variant deletion). Model relates to Fig 4bd.

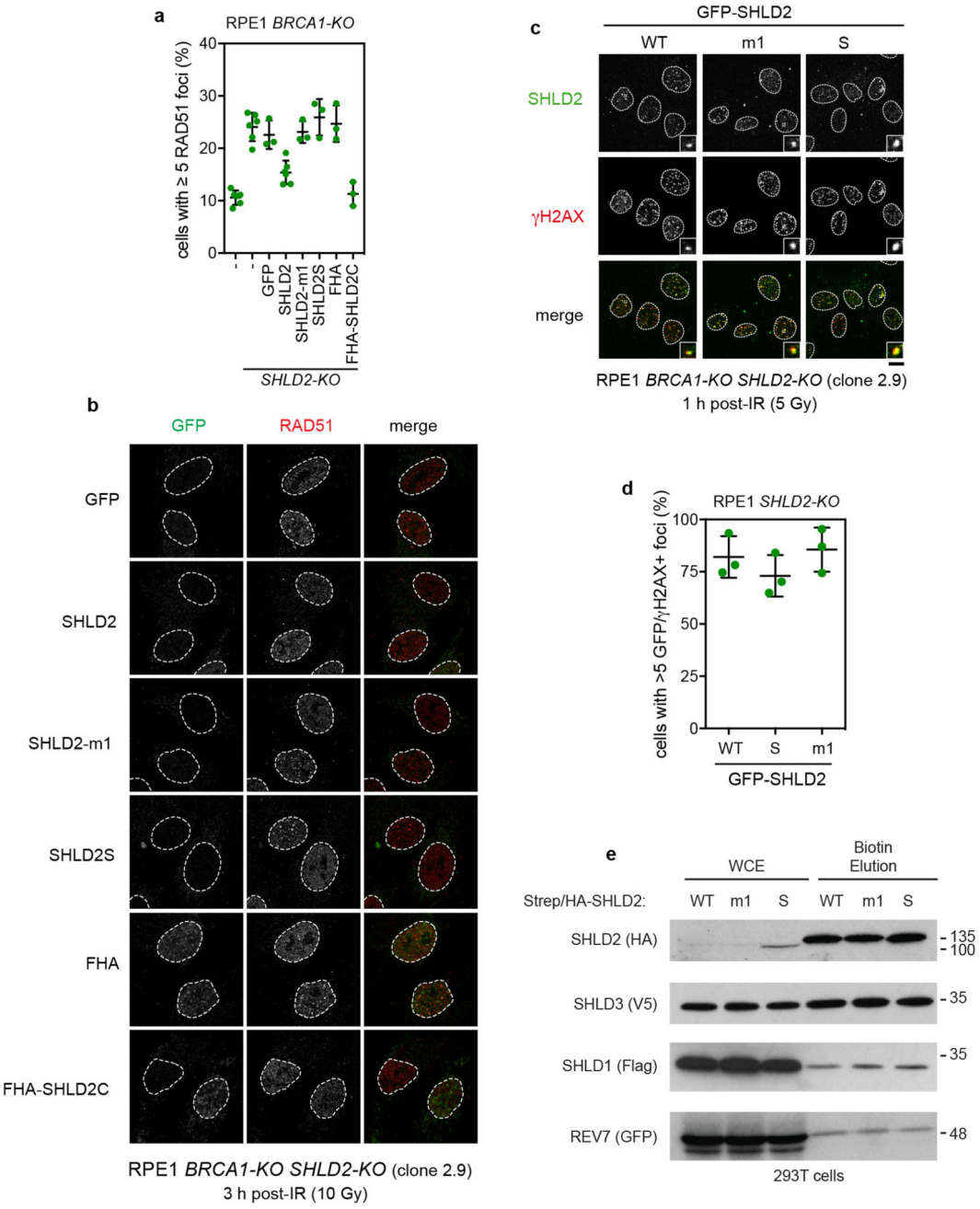

ED Figure 10. SHLD2 OB-folds are required for suppression of RAD51 IR-induced focus formation.

a, Quantitation of RAD51 foci 3 h following 10 Gy irradiation in RPE1 *BRCA1-KO/ SHLD2-KO* cells complemented with the indicated GFP-tagged SHLD2 constructs via viral transduction. Protein expression was induced with 1 μg/mL doxycycline for 24 h prior to IR. Each data point is a biological replicate; the bar represents the mean ± SD (n=6 for *BRCA1-KO* untransduced cells, *BRCA1-KO / SHLD2-KO* untransduced and GFP-SHLD2 cells, n=3 for remaining cell lines, biologically independent experiments). **b,** Representative

micrographs of the data shown in ED Fig 10a. Note that due to the pre-extraction required for visualization of RAD51 foci, the visualization of non-FHA tagged SHLD2 foci is lost. **c,** Representative micrographs of RPE1 *BRCA1-KO/SHLD2-KO* cells virally transduced with vectors expressing GFP-tagged SHLD2 WT or its OB-fold m1 mutant (m1), or short splice variant (S), 1 h post 5 Gy IR. Scale bar = 10 μm. **d,** Quantitation of the data shown in ED Fig 10c. Each data point represents an independent biological replicate counting ≥100 cells. Data is represented as mean ± SD (n=3). **e,** Whole cell extracts (WCE) of 293T cells co-transfected with Strep/HA-SHLD2 WT, -SHLD2-m1, or -SHLD2-S mutants, and other Shieldin subunits (Flag-SHLD1, V5-SHLD3, and GFP-REV7) were incubated with streptavidin resin and bound proteins were eluted with biotin. WCEs and eluted proteins were visualized by SDS-PAGE and immunoblotting with the indicated antibodies. Results shown are a representative set from 2 independent experiments.

Supplementary Material

Refer to Web version on PubMed Central for supplementary material.

Acknowledgments

We thank J. Young (Repare Therapeutics), M. Bashkurov (NBCC, LTRI), L. Kesselman (LTRI), S. Rossi (LTRI) and M. Rother (LUMC). We thank R. Greenberg (U Penn) for the U2OS-FokI cells. The authors acknowledge that J. Lukas first proposed the name Shieldin. SN is funded by a research fellowship from the Dutch Cancer Society (KWF). SAd is a Banting Post-Doctoral Fellow. DS is funded by a post-doctoral research fellowship from CIHR. HvA is funded by the European Research Council (CoG-50364). TH is supported by MD Anderson Cancer Center Support Grant P30 CA016672 and the Cancer Prevention Research Institute of Texas (CPRIT/RR160032). Work in the AM lab is funded through CIHR grant PJT153307. ACG is funded by CIHR grant FDN143301. Work in the CJL lab is funded by Programme Grants from Cancer Research UK (CRUK/A14276) and Breast Cancer Now (CTR-Q4-Y2). Work in the SR and JJ labs is funded by the Dutch Cancer Society (KWF 2014-6532), the Netherlands Organization for Scientific Research (VICI 91814643 and a National Roadmap grant for Large-Scale Research Facilities to JJ), the Swiss National Science Foundation (310030_156869 to SR), the European Research Council (CoG-681572 to SR and SyG-319661 to JJ). DD and ACG are Canada Research Chairs (Tier I). DD is funded by CIHR grant FDN143343, Canadian Cancer Society (CCS grant #705644) and OICR grant OICR-OC-TRI.

References

1. Panier S, Boulton SJ. Double-strand break repair: 53BP1 comes into focus. Nat Rev Mol Cell Biol. 2014; 15:7–18. DOI: 10.1038/nrm3719 [PubMed: 24326623]
2. Hustedt N, Durocher D. The control of DNA repair by the cell cycle. Nat Cell Biol. 2016; 19:1–9. DOI: 10.1038/ncb3452 [PubMed: 28008184]
3. Munoz IM, Jowsey PA, Toth R, Rouse J. Phospho-epitope binding by the BRCT domains of hPTIP controls multiple aspects of the cellular response to DNA damage. Nucleic acids research. 2007; 35:5312–5322. DOI: 10.1093/nar/gkm493 [PubMed: 17690115]
4. Zimmermann M, Lottersberger F, Buonomo SB, Sfeir A, de Lange T. 53BP1 Regulates DSB Repair Using Rif1 to Control 5' End Resection. Science. 2013; science.1231573 [pii]. doi: 10.1126/science.1231573
5. Feng L, Fong KW, Wang J, Wang W, Chen J. RIF1 counteracts BRCA1-mediated end resection during DNA repair. The Journal of biological chemistry. 2013; 288:11135–11143. DOI: 10.1074/jbc.M113.457440 [PubMed: 23486525]
6. Escribano-Diaz C, et al. A Cell Cycle-Dependent Regulatory Circuit Composed of 53BP1-RIF1 and BRCA1-CtIP Controls DNA Repair Pathway Choice. Molecular cell. 2013; 49:872–883. DOI: 10.1016/j.molcel.2013.01.001 [PubMed: 23333306]
7. Di Virgilio M, et al. Rif1 Prevents Resection of DNA Breaks and Promotes Immunoglobulin Class Switching. Science. 2013; science.1230624 [pii]. doi: 10.1126/science.1230624

8. Chapman JR, et al. RIF1 Is Essential for 53BP1-Dependent Nonhomologous End Joining and Suppression of DNA Double-Strand Break Resection. Mol Cell. 2013; S1097-2765(13)00003-8 [pii]. doi: 10.1016/j.molcel.2013.01.002
9. Callen E, et al. 53BP1 Mediates Productive and Mutagenic DNA Repair through Distinct Phosphoprotein Interactions. Cell. 2013; 153:1266–1280. DOI: 10.1016/j.cell.2013.05.023 [PubMed: 23727112]
10. Xu G, et al. REV7 counteracts DNA double-strand break resection and affects PARP inhibition. Nature. 2015; doi: 10.1038/nature14328
11. Boersma V, et al. MAD2L2 controls DNA repair at telomeres and DNA breaks by inhibiting 5' end resection. Nature. 2015; doi: 10.1038/nature14216
12. Fradet-Turcotte A, et al. 53BP1 is a reader of the DNA-damage-induced H2A Lys 15 ubiquitin mark. Nature. 2013; 499:50–54. DOI: 10.1038/nature12318 [PubMed: 23760478]
13. Adkins NL, Niu H, Sung P, Peterson CL. Nucleosome dynamics regulates DNA processing. Nature structural & molecular biology. 2013; 20:836–842. DOI: 10.1038/nsmb.2585
14. Jaspers JE, et al. Loss of 53BP1 causes PARP inhibitor resistance in Brca1-mutated mouse mammary tumors. Cancer discovery. 2013; 3:68–81. DOI: 10.1158/2159-8290.CD-12-0049 [PubMed: 23103855]
15. Bouwman P, et al. 53BP1 loss rescues BRCA1 deficiency and is associated with triple-negative and BRCA-mutated breast cancers. Nat Struct Mol Biol. 2010; 17:688–695. nsmb.1831 [pii]. DOI: 10.1038/nsmb.1831 [PubMed: 20453858]
16. Bunting SF, et al. 53BP1 inhibits homologous recombination in Brca1-deficient cells by blocking resection of DNA breaks. Cell. 2010; 141:243–254. S0092-8674(10)00285-0 [pii]. DOI: 10.1016/j.cell.2010.03.012 [PubMed: 20362325]
17. Lord CJ, Ashworth A. PARP inhibitors: Synthetic lethality in the clinic. Science. 2017; 355:1152–1158. DOI: 10.1126/science.aam7344 [PubMed: 28302823]
18. Pettitt SJ, et al. Genome-wide and high-density CRISPR-Cas9 screens identify point mutations in PARP1 causing PARP inhibitor resistance. bioRxiv. 2017; doi: 10.1101/203224
19. Hutchins JR, et al. Systematic analysis of human protein complexes identifies chromosome segregation proteins. Science. 2010; 328:593–599. DOI: 10.1126/science.1181348 [PubMed: 20360068]
20. Marechal A, Zou L. RPA-coated single-stranded DNA as a platform for post-translational modifications in the DNA damage response. Cell research. 2014; doi: 10.1038/cr.2014.147
21. Baumann P, Price C. Pot1 and telomere maintenance. FEBS Lett. 2010; 584:3779–3784. DOI: 10.1016/j.febslet.2010.05.024 [PubMed: 20493859]
22. Kuhar R, et al. Novel fluorescent genome editing reporters for monitoring DNA repair pathway utilization at endonuclease-induced breaks. Nucleic Acids Res. 2014; 42:e4.doi: 10.1093/nar/gkt872 [PubMed: 24121685]
23. Liu X, et al. Somatic loss of BRCA1 and p53 in mice induces mammary tumors with features of human BRCA1-mutated basal-like breast cancer. P Natl Acad Sci USA. 2007; 104:12111–12116. DOI: 10.1073/pnas.0702969104
24. Nakamura M, et al. High frequency class switching of an IgM+ B lymphoma clone CH12F3 to IgA + cells. Int Immunol. 1996; 8:193–201. [PubMed: 8671604]
25. Luijsterburg MS, et al. PARP1 Links CHD2-Mediated Chromatin Expansion and H3.3 Deposition to DNA Repair by Non-homologous End-Joining. Mol Cell. 2016; 61:547–562. DOI: 10.1016/j.molcel.2016.01.019 [PubMed: 26895424]
26. Mirman Z, et al. 53BP1/Rif1/Shieldin counteract DSB resection through CST/Polα-dependent fill-in. Nature. 2018 in press.
27. Fan J, Pavletich NP. Structure and conformational change of a replication protein A heterotrimer bound to ssDNA. Genes Dev. 2012; 26:2337–2347. DOI: 10.1101/gad.194787.112 [PubMed: 23070815]
28. Hanafusa T, et al. Overlapping in short motif sequences for binding to human REV7 and MAD2 proteins. Genes Cells. 2010; 15:281–296. DOI: 10.1111/j.1365-2443.2009.01380.x [PubMed: 20088965]

29. Sanjana NE, Shalem O, Zhang F. Improved vectors and genome-wide libraries for CRISPR screening. Nat Methods. 2014; 11:783–784. DOI: 10.1038/nmeth.3047 [PubMed: 25075903]
30. Shalem O, et al. Genome-scale CRISPR-Cas9 knockout screening in human cells. Science. 2014; 343:84–87. DOI: 10.1126/science.1247005 [PubMed: 24336571]
31. Olhovsky M, et al. OpenFreezer: a reagent information management software system. Nat Methods. 2011; 8:612–613. DOI: 10.1038/nmeth.1658 [PubMed: 21799493]
32. Elstrodt F, et al. BRCA1 mutation analysis of 41 human breast cancer cell lines reveals three new deleterious mutants. Cancer Res. 2006; 66:41–45. DOI: 10.1158/0008-5472.CAN-05-2853 [PubMed: 16397213]
33. Brinkman EK, Chen T, Amendola M, van Steensel B. Easy quantitative assessment of genome editing by sequence trace decomposition. Nucleic Acids Res. 2014; 42:e168.doi: 10.1093/nar/gku936 [PubMed: 25300484]
34. Bouwman P, et al. A high-throughput functional complementation assay for classification of BRCA1 missense variants. Cancer Discov. 2013; 3:1142–1155. DOI: 10.1158/2159-8290.CD-13-0094 [PubMed: 23867111]
35. Duarte AA, et al. BRCA-deficient mouse mammary tumor organoids to study cancer-drug resistance. Nat Methods. 2017; doi: 10.1038/nmeth.4535
36. Hart T, et al. High-Resolution CRISPR Screens Reveal Fitness Genes and Genotype-Specific Cancer Liabilities. Cell. 2015; 163:1515–1526. DOI: 10.1016/j.cell.2015.11.015 [PubMed: 26627737]
37. Li W, et al. MAGeCK enables robust identification of essential genes from genome-scale CRISPR/Cas9 knockout screens. Genome Biol. 2014; 15:554.doi: 10.1186/s13059-014-0554-4 [PubMed: 25476604]
38. Tzelepis K, et al. A CRISPR Dropout Screen Identifies Genetic Vulnerabilities and Therapeutic Targets in Acute Myeloid Leukemia. Cell Rep. 2016; 17:1193–1205. DOI: 10.1016/j.celrep.2016.09.079 [PubMed: 27760321]
39. Hart T, et al. Evaluation and Design of Genome-Wide CRISPR/SpCas9 Knockout Screens. G3 (Bethesda). 2017; 7:2719–2727. DOI: 10.1534/g3.117.041277 [PubMed: 28655737]
40. Wang G, et al. Identifying drug-gene interactions from CRISPR knockout screens with drugZ. bioRxiv. 2017; doi: 10.1101/232736
41. Tkac J, et al. HELB Is a Feedback Inhibitor of DNA End Resection. Mol Cell. 2016; doi: 10.1016/j.molcel.2015.12.013
42. Shteynberg D, et al. iProphet: multi-level integrative analysis of shotgun proteomic data improves peptide and protein identification rates and error estimates. Mol Cell Proteomics. 2011; 10 M111 007690. doi: 10.1074/mcp.M111.007690
43. Liu G, et al. ProHits: integrated software for mass spectrometry-based interaction proteomics. Nature biotechnology. 2010; 28:1015–1017. DOI: 10.1038/nbt1010-1015
44. Choi H, et al. SAINT: probabilistic scoring of affinity purification-mass spectrometry data. Nature methods. 2011; 8:70–73. DOI: 10.1038/nmeth.1541 [PubMed: 21131968]
45. Teo G, et al. SAINTexpress: improvements and additional features in Significance Analysis of INTeractome software. Journal of proteomics. 2014; 100:37–43. DOI: 10.1016/j.jprot.2013.10.023 [PubMed: 24513533]
46. Mellacheruvu D, et al. The CRAPome: a contaminant repository for affinity purification-mass spectrometry data. Nat Methods. 2013; 10:730–736. DOI: 10.1038/nmeth.2557 [PubMed: 23921808]
47. Tang J, et al. Acetylation limits 53BP1 association with damaged chromatin to promote homologous recombination. Nature structural & molecular biology. 2013; doi: 10.1038/nsmb.2499
48. Koo BK, et al. Controlled gene expression in primary Lgr5 organoid cultures. Nat Methods. 2011; 9:81–83. DOI: 10.1038/nmeth.1802 [PubMed: 22138822]
49. Drean A, et al. Modeling Therapy Resistance in BRCA1/2-Mutant Cancers. Mol Cancer Ther. 2017; 16:2022–2034. DOI: 10.1158/1535-7163.MCT-17-0098 [PubMed: 28619759]

Europe PMC Funders Author Manuscripts

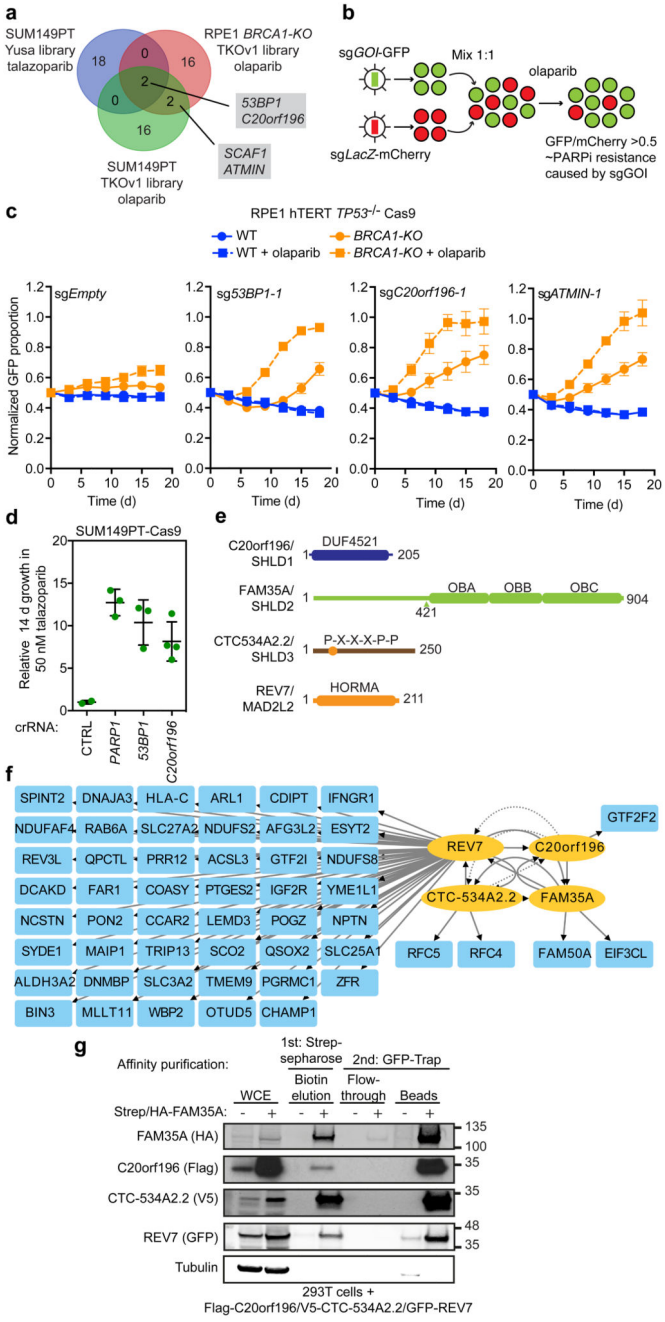

Figure 1. Identification of Shieldin.

a, Venn diagram of the top 20 hits in each screen. **b**, Schematic of the competitive growth assays. **c,** Competitive growth assays ± olaparib (16 nM) in RPE1 *BRCA1-KO* cells. Data represents mean fraction of GFP positive cells ± SEM, normalized to day 0 (n = 3, independent transductions). **d,** PARPi resistance caused by mutation of *C20orf196*. SUM149PT cells transfected with indicated crRNAs were treated with 50 nM talazoparib for 14 d. Relative growth was normalized to a non-targeting crRNA (CTRL). Bars represent mean ± SD of multiple crRNAs per gene (shown is a representative plot of 2 biologically

independent experiments). **e,** Domain architecture of Shieldin subunits. SHLD3 contains a REV7-binding PXXXPP motif28. **f,** Protein interaction network surrounding REV7, C20orf196, FAM35A and CTC-534A2.2. Solid and dashed arrows represent interactions at an FDR of ≤1% and ≤5%, respectively. **g,** Sequential affinity purifications from 293T cell lysates expressing the indicated proteins. Bound proteins were immunoblotted with the indicated antibodies (n = 2 independent experiments).

Europe PMC Funders Author Manuscripts

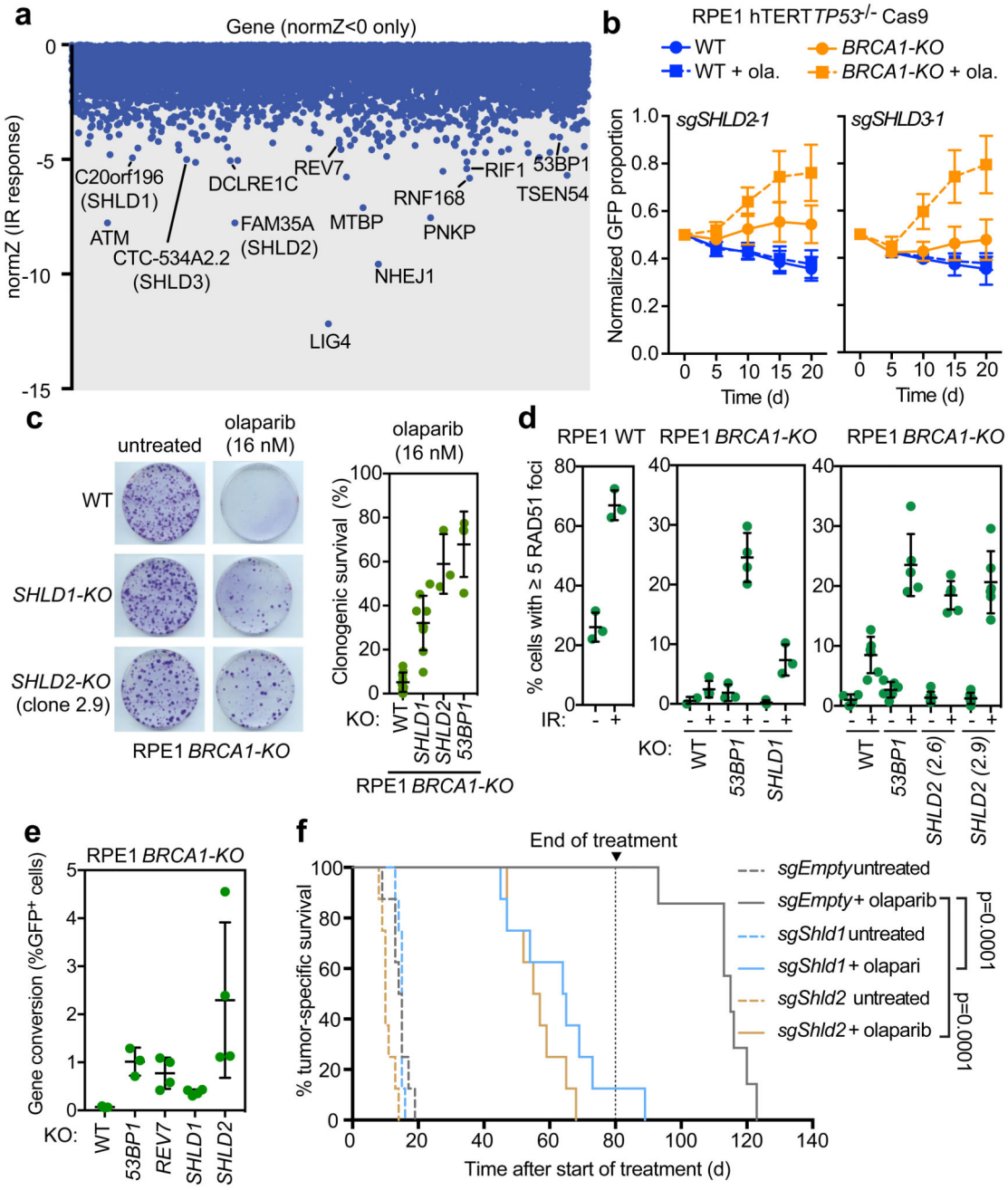

Figure 2. Shieldin loss promotes PARPi resistance in cell and tumor models of *BRCA1*-deficiency.

a, CRISPR dropout screen results in RPE1 WT cells exposed to IR. Shown are gene-level normZ scores <0. **b,** Competitive growth assays using olaparib (16 nM) in RPE1 *BRCA1-KO* cells. Data is presented as mean ± SD, normalized to day 0 (n = 3, independent transductions). **c** Clonogenic survival in response to 16 nM olaparib. Representative images are shown (left) and quantified (right). Bars represent mean ± SD (n=9: RPE1 WT and *BRCA1-KO SHLD1-KO*; n=3: *BRCA1-KO SHLD2-KO*, n=4: *BRCA1-KO 53BP1-KO*; biologically independent experiments). **d,** Quantitation of cells with ≥5 RAD51 foci ± 10 Gy

IR (6 h recovery). Biologically independent experiments are shown and the bar represents the mean ± SD. From left to right, the number of replicates was n=3 and n=3 (left panel); n=3, n=4, n=3, n=4, n=3 and n=3 (middle panel); and n=4, n=6, n=6, n=6, n=6, n=6, n= 6 and n=6 (right panel) **e,** Assessment of gene conversion by traffic light reporter assay. Biologically independent experiments are shown and the bar represents the mean ± SD (n=3 for WT and *53BP1-KO*; n=4 for *SHLD1-KO, SHLD2-KO,* and *REV7-KO*). **f,** Kaplan-Meier curve showing tumor-specific survival of mice transplanted with KB1P4 tumor organoids ± olaparib treatment for 80 d (n = 8 per treatment; editing efficiencies found in Supplementary Table 2). P-values were calculated using a log-rank test (Mantel-Cox).

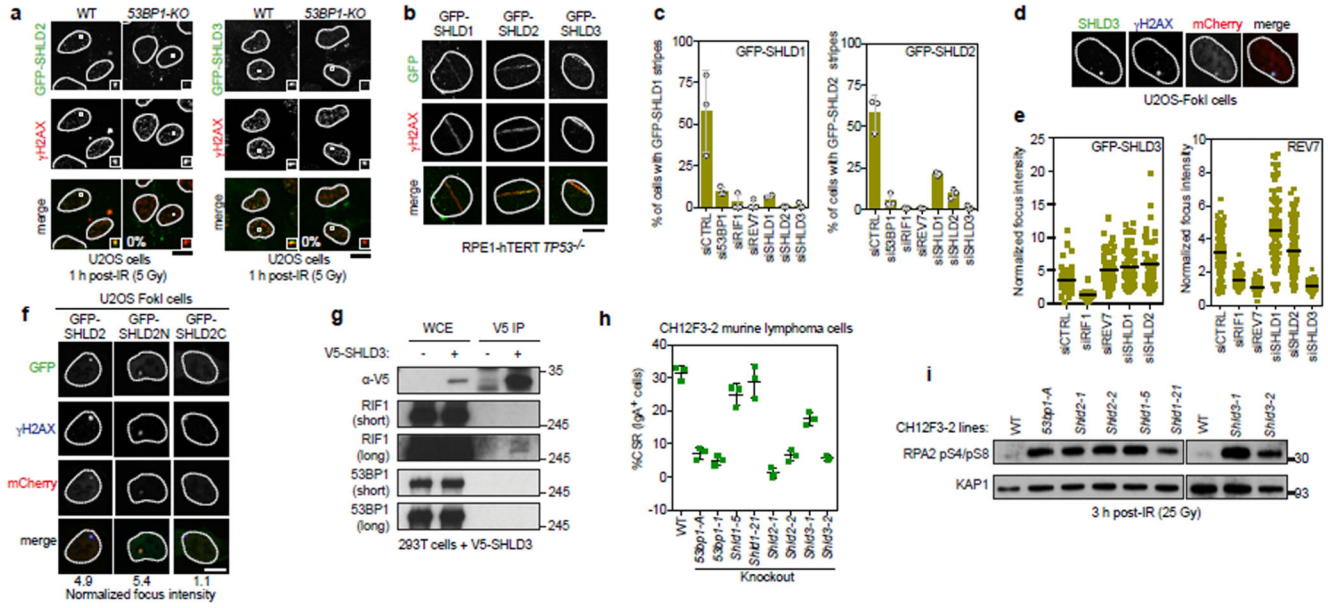

Figure 3. Shieldin accumulates at DSB sites downstream of 53BP1-RIF1 and promotes class switch recombination.

a-b, Representative micrographs of Shieldin subunit accumulation into IR-induced foci in U2OS cells (a) or at laser-microirradiation sites in RPE1 cells (b) (n=3 biologically independent experiments). **c,** Quantitation of (b). Points represent individual experiments counting ≥100 cells. Bar represents mean ± SD. **d,** Colocalization of GFP-tagged Shieldin subunits with mCherry foci in U2OS-FokI cells upon mCherry-LacR-FokI expression. **e,** Quantitation of GFP-SHLD3 or endogenous REV7 focus intensity. Each point represents a cell. Line represents the mean. Data is the aggregate of two biological replicates with a total of 50 and 120 (GFP-SHLD3 and REV7, respectively), 45 and 122, 48 and 112, 54 and 116, 49 and 111, and 117 cells counted for siCTRL, siRIF1, siREV7, siSHLD1, siSHLD2 and siSHLD3, respectively. **f,** mCherry-LacR-FokI colocalization with GFP-SHLD2, SHLD2N, and SHLD2C. Mean normalized focus intensity is shown with a total of 52 (SHLD2 and SHLD2N) or 53 (SHLD2C) cells counted (n=2, biologically independent experiments). **g**, RIF1 co-immunoprecipitation with V5-SHLD3 (representative of two independent experiments). **h,** CSR analysis of CH12F3-2 cells following stimulation. Data is represented as the mean ± SD (n=3 biologically independent replicates). **i,** Irradiated (25 Gy) CH12F3-2 clones were immunoblotted for RPA2 phosphorylation (representative of three biological replicates).

Europe PMC Funders Author Manuscripts

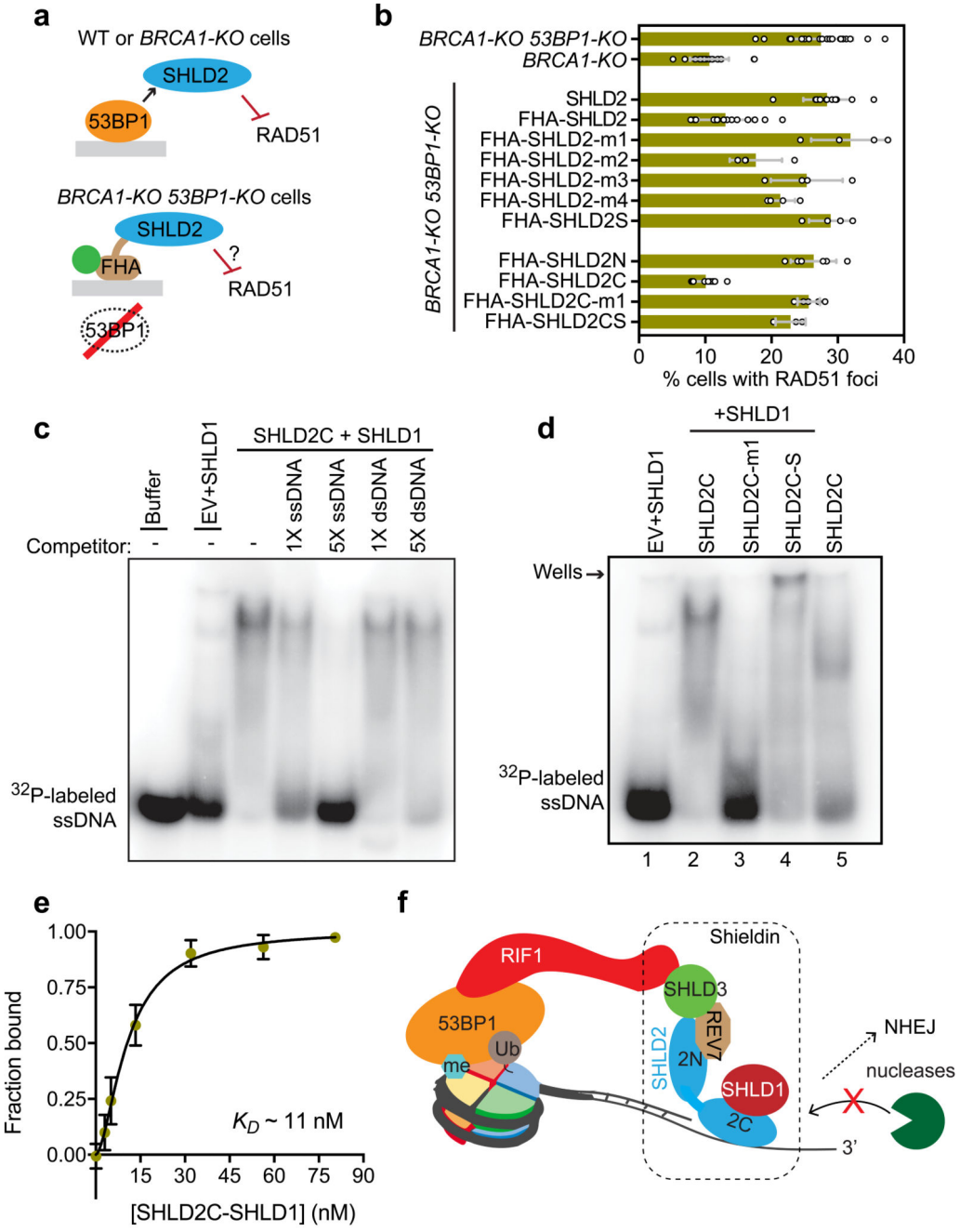

Figure 4. Shieldin is an effector of 53BP1 by binding ssDNA.

a, Schematic for artificially targeting Shieldin to DSB sites. **b**, RAD51 IRIF formation 3 h following 10 Gy irradiation in *BRCA1-KO 53BP1-KO* cells expressing the indicated fusion proteins. The bar represents the mean ± SD. From top to bottom the number of biologically independent experiments was n=20, n=22, n=12, n=12, n=16, n=4, n=4, n=4, n=4, n=4, n=6, n=6 and n=3. **c,** EMSA of the SHLD2C-SHLD1 complex isolated from 293T cells (see ED Fig 9b) incubated with radiolabeled ssDNA ± unlabelled oligonucleotides (n=2 independent experiments). EV refers to empty vector. **d,** EMSA of SHLD2C WT and variants (n=4

Europe PMC Funders Author Manuscripts

independent experiments). **e,** Determination of SHLD2C-SHLD1 ssDNA binding dissociation constant (K_d). Mean values are presented ± SD (n=3 independent experiments). Representative EMSA shown in ED Fig 9c. **f,** Model of Shieldin function. We speculate that the SHLD2 OB-fold domains bind to ssDNA at DSB sites to suppress resection and favour NHEJ.

Europe PMC Funders Author Manuscripts